1992-12

C-Vector derived three dimensional circulations in Farallones National Marine Sanctuary.

Konstantinidis, Simon

Monterey, California. Naval Postgraduate School

NAVAL POSTGRADUATE SCHOOL

Monterey, California

THESIS

C-VECTOR DERIVED THREE DIMENSIONAL CIRCULATIONS IN FARALLONES NATIONAL MARINE SANCTUARY

by
Simon Konstantinidis

December, 1992

Thesis Advisor: P. C. Chu

REPORT DOCUMENTATION PAGE

1a. REPORT SECURITY CLASSIFICATION Unclassified	1b. RESTRICTIVE MARKINGS
2a. SECURITY CLASSIFICATION AUTHORITY	3. DISTRIBUTION/AVAILABILITY OF REPORT Approved for public release; distribution is unlimited.
2b. DECLASSIFICATION/DOWNGRADING SCHEDULE	
4. PERFORMING ORGANIZATION REPORT NUMBER(S)	5. MONITORING ORGANIZATION REPORT NUMBER(S)
6a. NAME OF PERFORMING ORGANIZATION Naval Postgraduate School 6b. OFFICE SYMBOL (*If applicable*) Oc	7a. NAME OF MONITORING ORGANIZATION Naval Postgraduate School Research Foundation
6c. ADDRESS (*City, State, and ZIP Code*) Monterey, CA 93943-5000	7b. ADDRESS (*City, State, and ZIP Code*) Monterey, CA 93943-5000
8a. NAME OF FUNDING/SPONSORING ORGANIZATION Naval Postgraduate School 8b. OFFICE SYMBOL (*If applicable*) Oc	9. PROCUREMENT INSTRUMENT IDENTIFICATION NUMBER
8c. ADDRESS (*City, State, and ZIP Code*) NPS Monterey Ca 93943	10. SOURCE OF FUNDING NUMBERS AC. ID 81CU2 2L000-2L999. 5076-50799 | JOB ORDER UHFD1

11 TITLE (*Include Security Classification*)
C-VECTOR DERIVED THREE DIMENSIONAL CIRCULATIONS IN THE FARALLONES NATIONAL MARINE SANCTUARY
UNCLASSIFIED

12. PERSONAL AUTHOR(S) Simon Konstantinidis

13a. TYPE OF REPORT	13b. TIME COVERED	14. DATE OF REPORT (*year, month, day*)	15. PAGE COUNT
Master's Thesis	From To	December 1992	97

16. SUPPLEMENTARY NOTATION
The views expressed in this thesis are those of the author and do not reflect the official policy or position of the Department of Defense or the U.S. Government.

17. COSATI CODES			18. SUBJECT TERMS (*continue on reverse if necessary and identify by block number*)
FIELD	GROUP	SUBGROUP	C-Vector method, Pseudo-vorticity fields in the Gulf of Farallones National Marine Sanctuary

19. ABSTRACT (*continue on reverse if necessary and identify by block number*)

Neglecting the ageostrophic circulation is not very realistic for the ocean circulation in coastal waters andparticularly in regions with strong temperature and salinity gradients like the Farallones Natinal Marine Sanctuary. The C-Vector method has been developed to diagnose the three dimensinal flow including ageostrophic circulation. This thesis uses the C-Vector concept and data collected from the R/V Point Sur in the area of Farallones National Marine Sanctuary in order to describe and illustrate the three dimensional pseudo-vorticity fields of the ageostrophic circulation and the total circulation (geostrophic and ageostrophic) of the region.

20. DISTRIBUTION/AVAILABILITY OF ABSTRACT	21. ABSTRACT SECURITY CLASSIFICATION	
☒ UNCLASSIFIED/UNLIMITED ☐ SAME AS REPORT ☐ DTIC USERS	Unclassified	
22a. NAME OF RESPONSIBLE INDIVIDUAL Peter C. Chu	22b. TELEPHONE (*Include Area code*) 408 656 - 3257	22c. OFFICE SYMBOL Oc/Cu

DD FORM 1473, 84 MAR 83 APR edition may be used until exhausted
All other editions are obsolete

Approved for public release; distribution is unlimited.

C-Vector Derived Three Dimensional Circulations
in Farallones National Marine Sanctuary
by
Simon Konstantinidis
Lieutenant, Hellenic Navy
B.S., Hellenic Naval Academy

Submitted in partial fulfillment
of the requirements for the degree of

MASTER OF SCIENCE IN PHYSICAL OCEANOGRAPHY AND METEOROLOGY

from the

NAVAL POSTGRADUATE SCHOOL
December 1992

ABSTRACT

Neglecting the ageostrophic circulation is not very realistic for ocean circulation in coastal waters and particularly in regions with strong temperature and salinity gradients like the Farallones National Marine Sanctuary. The C-Vector method has been developed to diagnose the three dimensional flow including ageostrophic circulation. This thesis uses the C-Vector method and data collected from the *R/V Point Sur* in the area of Farallones National Marine Sanctuary in order to describe and illustrate the three dimensional pseudo-vorticity fields of the ageostrophic circulation and the total circulation (geostophic and ageostrophic) of the region.

TABLE OF CONTENTS

LIST OF TABLES

LIST OF FIGURES

ACKNOWLEDGEMENTS

I would like to thank my thesis advisor Dr. P. Chu whose professional guidance, patience, and support has been an essential and invaluable part of my thesis.

I would like also to thank the Chairman of the Oceanography Department Dr. C. Collins for providing the data, Dr. R. W. Garwood for being my second reader, Dr. N. Garfield for providing a satellite picture, Oceanographer P. Jessen for assisting me in plotting and correcting syntactical errors in my thesis and Miss M. Orpilla for typing my thesis.

I. INTRODUCTION

A. GULF OF THE FARALLONES NATIONAL MARINE SANCTUARY

1. Geophysical Characteristics

The boundaries of the Farallones shelf and slope region extend from Point Ano Nuevo on the south to Point Reyes on the north and westward from 10 km to 90 km off shore.

This continental margin, which includes the coastal zone off San Francisco and is characterized by a shelf with a maximum width of 45 km, is the widest shelf along the entire

Figure 1. Continental margin profile in the vicinity of Santa Cruz mountains (Shepard, 1941).

west coast of the United States (Figure 1). This is, however, narrower than most of the shelves off the eastern and southern coasts of the United States. The shelf width reduces gradually to the north. Another characteristic that distinguishes the region is that the submarine canyons are

almost completely limited to the continental slope, beginning well out from the coast.

West of Point Ano Nuevo, the direction of the continental slope veers northwest. The steepest part of the slope branches away from the shelf border north of latitude 37^0 and a relatively smooth gradient extends to depths of 1,000 to or 1,300 m. West of the Farallones Islands, the steepest zone is close to the shelf margin, but farther north and beyond Cordell Bank, there is a circular shape to the upper limit of the continental slope.

The fact that most canyons are restricted to the continental slope in this region may have some bearing on the relatively smooth character of the upper parts of this slope (Figure 2). However, there are many canyons on the outer slope. One of these canyons is the Pioneer Canyon between stations 8, 9 and 10 of section A and stations 11, 12 and 13 of Section B. The maximum depth of this canyon is about 3,400 m between stations 10 and 11 (Figure 3).

According to earlier studies (Stetson, 1936 and Shepard *et al.* 1941), currents in canyons might alternate in direction, but more often the strongest currents are down the canyon. It was thought in these early studies that the period of alternation was not tidal.

Shepard *et al.*, (1979) believed that in areas with small tidal ranges, where short period alternations occur at

considerable depth, the tidal current oscillations are subordinate to regional current oscillations at other frequencies.

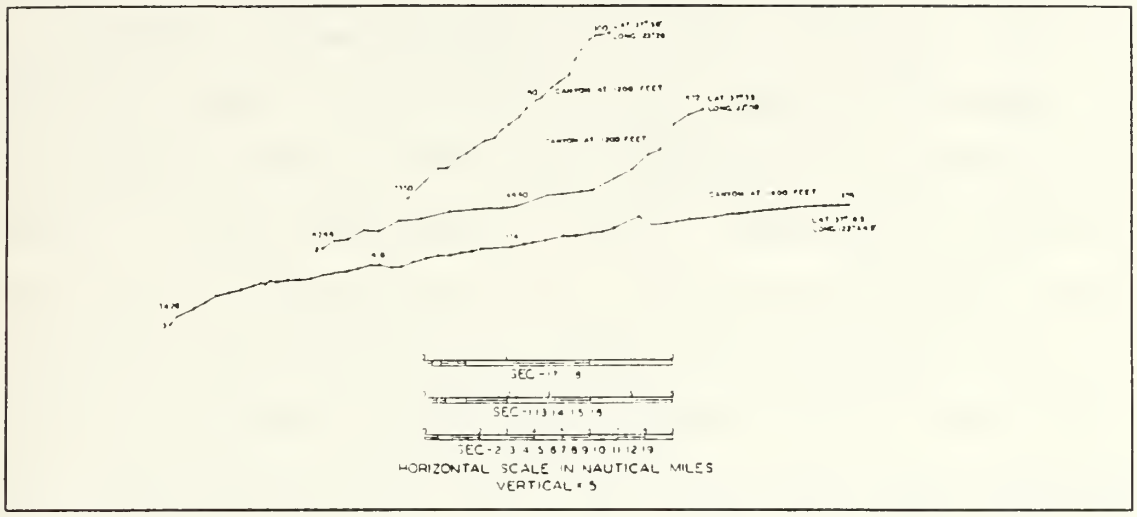

Figure 2.Profiles down the main submarine canyons off San Francisco (Shepard, 1941).

An oval seamount, the Pioneer Seamount lies northwest of Pioneer Canyon and southwest of Farallones Islands. South of Pioneer Canyon is another oval seamount, Guide Seamount. Both rise about 1,000 m above the sea floor at the base of the slope, and each has more than one summit. These features may also play an important role in the water circulation and the currents of the region.

2. Water Masses

To study the water masses of the Farallones National Marine Sanctuary, the characteristic water masses in the North Pacific which may influence the currents west of San Francisco must be analyzed.

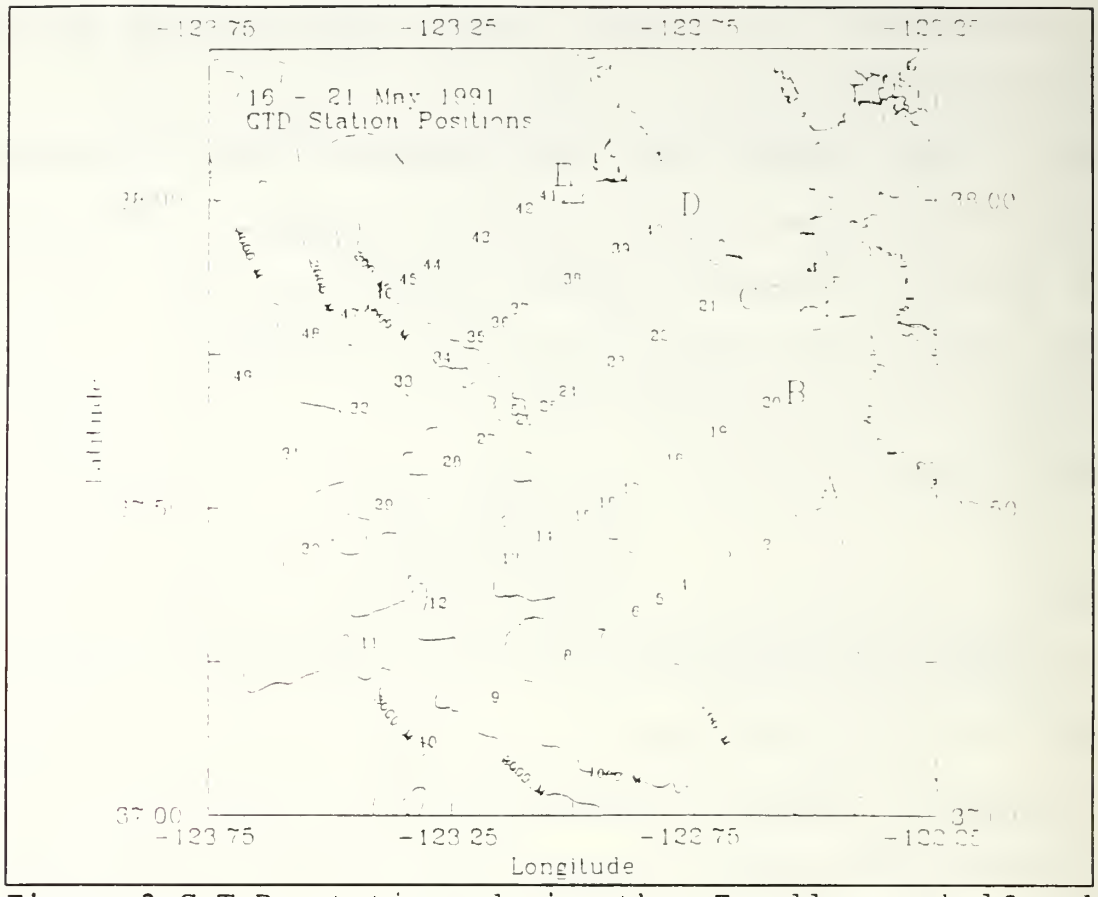

Figure 3 C.T.D. stations during the Farallones shelf and slope study.

According to Sverdrup *et al.* (1964) the water mass which dominates the upper waters of the North Pacific is the subarctic water mass. The subarctic water mass is characterized as the water mass northward of latitude 45^0 North. For the sake of convenience, this name is used for the entire water mass above the latitude of 23^0 North. This water mass is advected eastward and then southward.

Between 22^0 and 45^0 and depths below 300 m, temperature and salinity (T-S) curves show waters intermediate in character between subarctic North Pacific and the Equatorial water. The water at the region of interest is formed by the mixing of these two large and well defined water masses. It was determined by Collins (1992) that a poleward penetration of Equatorial water (associated with the under currents) occurred along shore over the continental slope at the Gulf of Farallones Islands between 16 and 21 May 1991. Also, the waters were found to be warm and fresh showing characteristics of subarctic waters (at station 48).

Sverdrup and Fleming (1941) and Tibby (1941) discovered that near the coast (30 km), the water mass had characteristics closer to the equatorial water mass than to subarctic water mass. It is obvious that close to the coast, the subarctic North Pacific water mass has less effect on than Equatorial Water mass characteristics.

According to Hickey (1979) the California Undercurrent is a northward subsurface flow off the west coast of North America over the continental slope. The main flow, which carries equatorial type water, was found at 200 m depth. During the Farallones shelf and slope study, the undercurrent had maximum observed velocities at a depth of 100 to 200 m.

It has a jet-like structure, both vertically and horizontally, and extends to the bottom over the slope.

The most permanent current of the shelf circulation during upwelling is the coastal jet which is a southward flow with a maximum speed located between 5 km and 25 km from the coast. Huyer *et al.* (1978) and Huyer *et al.* (1975) found that the seasonally averaged jet is stronger during the spring than in the summer.

According to Yoshida (1967), "processes near coastal boundaries respond greater and faster to time variable winds than those in the central oceans." During the first two weeks of September 1979, there were weak westerly winds which were not favorable for the maintenance of strong upwelling. At that period Breaker and Gillilard (1981) used IR images from the Advanced Very High Resolution Radiometer (AVHRR) to show the upwelled waters, near San Francisco, enter and leave San Francisco Bay. From the observed time sequences the upwelled waters appear to reflect the strong tidal influence at this location (Conomos, 1979).

The Davidson current which is a northward near-shore flow is commonly observed north of Point Conception during the winter months (Reid *et al.*, 1958), but can occur in other seasons under favorable wind conditions (Wyatt *et al.*, 1972). The fact that drift bottles released north of Point Conception have been recovered as far north as Vancouver Island

(Schwartzlose, 1963; Crowe and Schwartzlose, 1972) is strong evidence that the flow is usually continuous alongshore.

The California Current (CC) which is more fully developed during spring and early summer has its core approximately 100 - 200 km offshore (Chelton, 1984) and for this reason, does not greatly affect the area of study which extends only 90 km off shore.

3. Weather Conditions

Weather conditions during the cruise are shown in Figure 4. The hourly averaged wind vectors are from west-northwest as usually happens during this season in this area (Huyer, 1983). The wind speed ranges from 3.8 to 17.2 m/sec and contributes to the upwelling process in the region. Air temperature is relatively low, between 9.8^0 C and 11.6^0 C.

B. GENERAL CLIMATOLOGICAL PICTURE

The data used in this thesis was gathered as part of an Environmental Protection Agency (EPA) funded plan to study oceanographic currents and hydrographic conditions in the area of the Gulf of the Farallones National Marine Sanctuary (Figure 3).

According to the schedule, five surveys were conducted. This survey was carried out between May 16 to 21, 1991 aboard the research vessel *Point Sur* and was the second survey of the five.

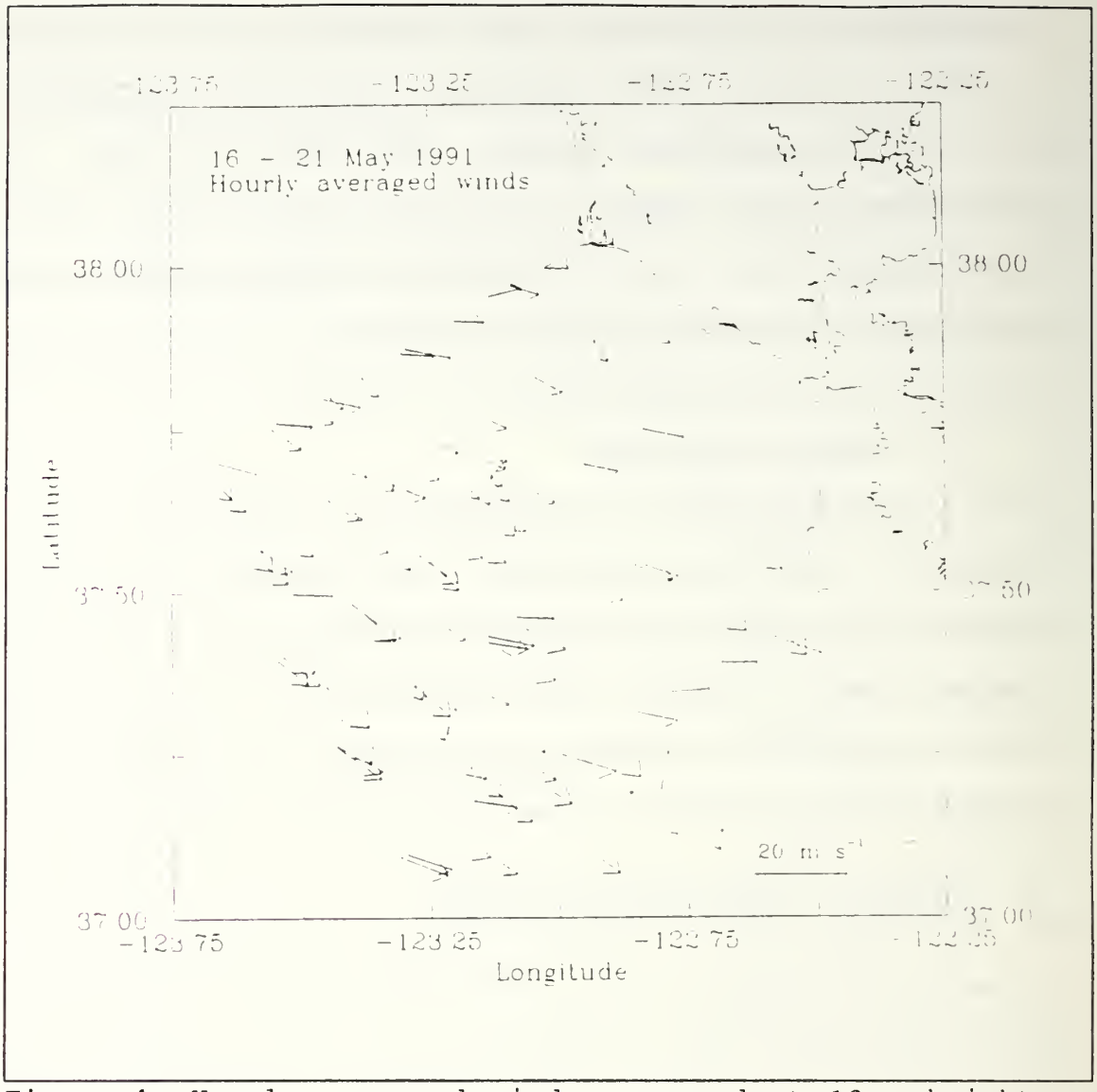

Figure 4. Hourly averaged winds measured at 10 m height on board *R/V Point Sur* during the cruise of May 16 - 21, 1991 (Jessen *et al.*, 1992).

During this cruise, a three-dimensional map of hydrographic data was obtained in order to better understand the currents of the area.

Additionally, data was acquired from Advanced Very High Resolution Radiometer (AVHRR or AVHRR/2) instruments on board

TIROS-N/NOAA polar orbiting satellite and interpreted as Sea Surface Temperature (SST) images.

Table I. ISLANDS, ROCKS AND SHOALS IN THE GULF OF THE FARALLONES NATIONAL MARINE SANCTUARY.

Islands , Rocks and Shoals	Latitude North		Longitude West	
1.S.E.Farallon Is.	37	42	123	00
2.Mid. Farallon Is.	37	44	123	0●
3.North Farallon Is.	37	46	123	0●
4.Fanny Shoal	37	47.5	123	10.5
5.Noonday Rock	37	47.5	123	●0
6.Hurst shoal	37	41.5	123	00
7.Maintop Is.	37	41.8	123	00

The locations of the Farallones Islands, rocks and shoals near stations 22, 23 of Section C and 37, 38 of Section D, are listed in Table I.

C. PURPOSE OF THE STUDY - CONTENTS

This research investigates the three-dimensional ageostrophic pseudo-vorticity fields and the pseudo-vorticity fields of the total circulation near continental shelves and slopes extracting the necessary information from the hydrographic and wind data sets (Figure 5).

The California Current (CC), which is the eastern part of the subtropical North Pacific gyre and extends from Washington State to Baja California, is the main current at the surface. The California Undercurrent or Inshore Current (IC) with poleward flow is the main current below the surface in this region. The geostrophic part of these currents can be directly obtained from the hydrographic data sets (CTD data sets).

The ageostrophic portion of these currents can be indirectly obtained by the C-Vector which can be calculated from hydrographic data and surface wind stress data.

In this thesis, Chapter II covers the C-Vector concept and the techniques for the C-Vector calculations. Chapter III describes instruments, methods and data processing techniques. Chapter IV provides detailed analysis of the plots of the C-Vector for the ageostrophic circulation and the C-Vector for the total circulation (geostrophic and ageostrophic).

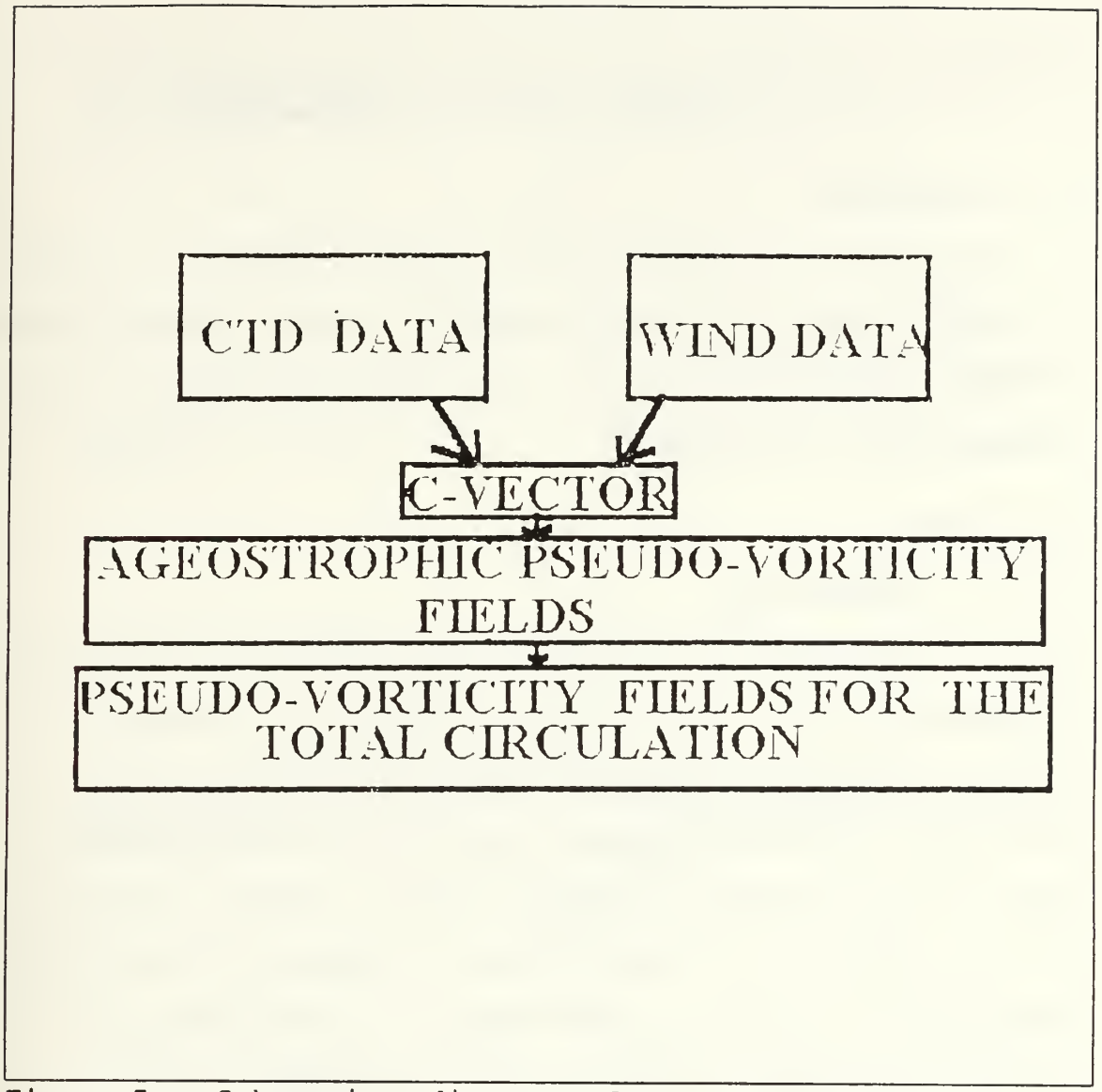

Figure 5. Schematic diagram for the calculation of ageostrophic pseudo-vorticity fields and then the pseudo-vorticity fields for the total circulation.

Finally, Chapter V summarizes the results and offers recommendations for future work.

II. C-VECTOR CONCEPT AND TECHNIQUES

A. OBJECTIVE

The main objective of the C-Vector concept is to compute a three-dimensional pseudo-vorticity fields from the density fields and its derivatives, and then to obtain a three-dimensional circulation.

B. THEORY

1. Meteorology

The general idea was first proposed for atmospheric circulation with the Q-vector concept of Hoskins *et al.* (1978). Hoskins *et al.* found that the Q-Vector was obtained from the ω-equation and can be explained on the synoptician's chart more precisely than in earlier studies (Sutcliffe, 1947). This theory is very helpful in diagnosing the synoptic and frontal vertical circulation. A disadvantage of this concept is that it ignores the barotropic part of the rotational ageostrophic flow. According to Xu (1992) this problem can be overcome by the C-Vector concept which resolves the ageostrophic circulation more conveniently and allows a new way of solving the C-Vector equation. The C-Vector equation is a three-dimensional extension of the Q-Vector equation (QG diagnostic equation).

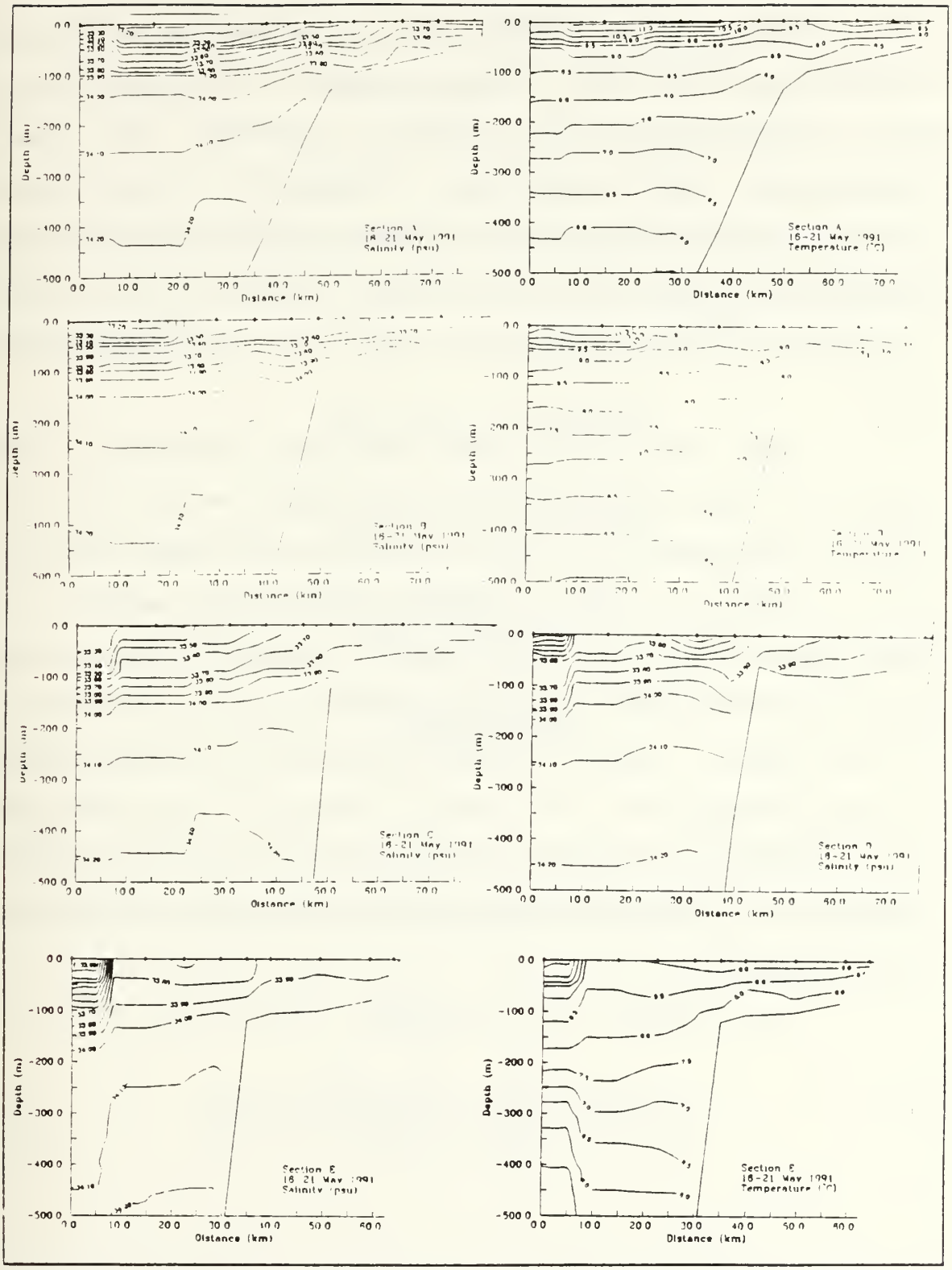

Figure 6. Vertical Temperature and Salinity plots (Jessen *et al.* 1992).

2. Physical Oceanography

The C-Vector concept can also be applied to oceanic circulation (Chu, 1992). With the help of this concept and a set of hydrographic and surface wind data, the three-dimensional pseudo-vorticity fields of ageostrophic circulation in the oceans are diagnosed. Also revealed are the three dimensional pseudo-vorticity fields of the total circulation which includes both geostrophic and ageostrophic flow.

Only CTD data are needed for this calculation of the currents, obviating a need for more expensive and difficult direct measurements of ocean currents in sufficient quantity.

There is never a perfect geostrophic balance. A geostrophic balance is traditionally assumed for calculation of the currents because the ageostrophic part is considered to be very small. However this assumption is of questionable validity especially for coastal waters of the Farallones National Marine Sanctuary where there are significant temperature and salinity gradients like the one at Section E and D (Figure 8).

The thermal wind equations,

$$\frac{\partial}{\partial z}(\rho f v_g) = -g\frac{\partial \rho}{\partial x} \quad , \quad \frac{\partial}{\partial z}(\rho f u_g) = g\frac{\partial \rho}{\partial y} \tag{1}$$

(where ρ is the sea water density, f is the Coriolis parameter $f=2\Omega\sin\phi$) are used for the calculation of the geostrophic currents (U_g, V_g). The geostrophic currents are not, however, the total currents. In order to have more realistic flow fields the ageostrophic circulation must be included. Following Chu (1992), the basic equations for coastal waters including ageostrophic circulation, wind stress and excluding buoyancy are:

$$\left(\frac{\partial}{\partial t}+\vec{V}\cdot\nabla\right) u-f(v-V_g)=\frac{\partial Y^x}{\partial z} \tag{2}$$

$$\left(\frac{\partial}{\partial t}+\vec{V}\cdot\nabla\right) v+f(u-U_g)=\frac{\partial Y^y}{\partial z} \tag{3}$$

$$\left(\frac{\partial}{\partial t}+\vec{V}\cdot\nabla\right) b+N^2 w=0 \tag{4}$$

$$\frac{\partial u}{\partial x}+\frac{\partial v}{\partial y}+\frac{\partial w}{\partial z}=0 \tag{5}$$

where N is the Brunt-Vaisala frequency (assuming N = constant), f is the Coriolis parameter (on an f - plane), V=(u,v,w), and (Y^y, Y^x) is the turbulent momentum flux due to surface wind stress (τ_x, τ_y),

$$Y^x|_{z=0}=\frac{\tau^x}{\rho_o} \quad , \quad Y^Y|_{z=0}=\frac{\tau^Y}{\rho_o} \tag{6}$$

The decomposition of the total current velocity into geostrophic velocity and ageostrophic circulation results in:

$$\vec{V} = \vec{V}_g + \vec{V}_a \tag{7}$$

Using the above equation (7) and after the decomposition of the basic equations (2) to (4), the system of equations will have the form,

$$\mathcal{H}(\vec{V}_a) = \mathfrak{R}(\vec{V}_g, \rho, Y^y, Y^x) \tag{8}$$

where $\mathcal{H}$, $\mathfrak{R}$ are specific differential operators. From functions $\mathcal{H}$ and $\mathfrak{R}$, the three-dimensional ageostrophic circulation can be calculated using equation (8) together with CTD and surface wind data.

3. Development of C-Vector equations (a Diagnostic System)

Equations (2) to (4), for coastal waters on an f - plane, can be decomposed using equation (7). The result will be the following equations:

$$-fv_a = \frac{\partial Y^x}{\partial z} - \left(\frac{\partial}{\partial t} + \vec{V}_g \cdot \nabla\right) U_g \tag{9}$$

$$fu_a = \frac{\partial Y^y}{\partial z} - \left(\frac{\partial}{\partial t} + \vec{V}_g \cdot \nabla\right) V_g \tag{10}$$

$$N^2 w_a = -\left(\frac{\partial}{\partial t} + \vec{V}_g \cdot \nabla\right) b \tag{11}$$

$$\frac{\partial u_a}{\partial x} + \frac{\partial v_a}{\partial y} + \frac{\partial w_a}{\partial z} = 0 \tag{12}$$

Taking the derivative of equation (9) with respect to z, and f times the derivative of equation (11) with respect to y, and adding them together (similarly working for equations (10) and (11)) results in the ageostrophic pseudo-vorticity equations:

$$-\frac{\partial}{\partial z}\left(f^2 v_a\right) + \frac{\partial}{\partial y}\left(N^2 w_a\right) = 2C_1 \tag{13}$$

$$\frac{\partial}{\partial z}\left(f^2 u_a\right) - \frac{\partial}{\partial x}\left(N^2 w_a\right) = 2C_2 \tag{14}$$

$$\frac{\partial}{\partial x}\left(f^2 v_a\right) - \frac{\partial}{\partial y}\left(f^2 u_a\right) = 2C_3 \tag{15}$$

where :

$$C_1 \equiv -f\left(\frac{\partial U_g}{\partial y}\frac{\partial V_g}{\partial z} - \frac{\partial V_g}{\partial y}\frac{\partial U_g}{\partial z}\right) + \frac{f}{2}\frac{\partial^2 Y^x}{\partial z^2} \tag{16}$$

$$C_2 \equiv -f\left(\frac{\partial U_g}{\partial z}\frac{\partial V_g}{\partial x} - \frac{\partial V_g}{\partial z}\frac{\partial U_g}{\partial x}\right) + \frac{f}{2}\frac{\partial^2 Y^y}{\partial z^2} \tag{17}$$

$$C_3 \equiv -f\left(\frac{\partial U_g}{\partial x}\frac{\partial V_g}{\partial y} - \frac{\partial V_g}{\partial x}\frac{\partial U_g}{\partial y}\right) - \frac{f}{2}\frac{\partial}{\partial z}\left(\frac{\partial Y^y}{\partial x} + \frac{\partial Y^y}{\partial y}\right) \tag{18}$$

$$\vec{C}_a \equiv (C_1, C_2, C_3) \tag{19}$$

The above equations yield the three components of the C_a - Vector. Having the C_a - Vector, the three dimensional ageostrophic circulation can be found.

Another important vector is the C-Vector (C_x, C_y, C_z) for the total flow, geostrophic and ageostrophic. The three components of this vector can be found with the following process.

Using equation (13) for the total flow ($v=v_g+v_a$ and $w=w_g+w_a$ but $w_g=0 \Rightarrow w=w_a$):

$$-\frac{\partial}{\partial z}(f^2 v) + \frac{\partial}{\partial y}(N^2 w) = -\frac{\partial}{\partial z}(f^2 v_a) - \frac{\partial}{\partial z}(f^2 v_g) + \frac{\partial}{\partial y}(N^2 w_a) = \tag{20}$$

$$= -\frac{\partial}{\partial z}(f^2 v_g) + 2C_1 \equiv 2C_x f^2 \Rightarrow \tag{21}$$

$$C_x \equiv \frac{C_1}{f^2} - \frac{1}{2}\frac{\partial v_g}{\partial z} \tag{22}$$

Working similarly, the other components can be found:

$$C_y \equiv \frac{C_2}{f^2} + \frac{1}{2}\frac{\partial u_g}{\partial z} \tag{23}$$

$$C_z \equiv \frac{C_3}{f^2} + \frac{1}{2}\left(\frac{\partial v_g}{\partial x} - \frac{\partial u_g}{\partial y}\right) \tag{24}$$

4. Physical Significance of C-Vector

There are two important physical meanings of C-Vector.

a. Direction of C-Vector

There is a non-dimensional formula which can appropriately show the relation between C-Vector and ageostrophic pseudo-vorticity :

$$\nabla\times\vec{V}_a=2R_0\vec{C} \tag{25}$$

$$\nabla\cdot\vec{V}_a=0 \tag{26}$$

where R_0 is the Rossby number ($R_0\equiv U/(fL)$).

Equation (25) shows that C-Vector is proportional to the ageostrophic vorticity. A C-Vector stream line can be considered as an ageostrophic vortex line (Figure 7).

b. Relation between w_a and vertical vorticity of C-Vector.

This relation can be found from:

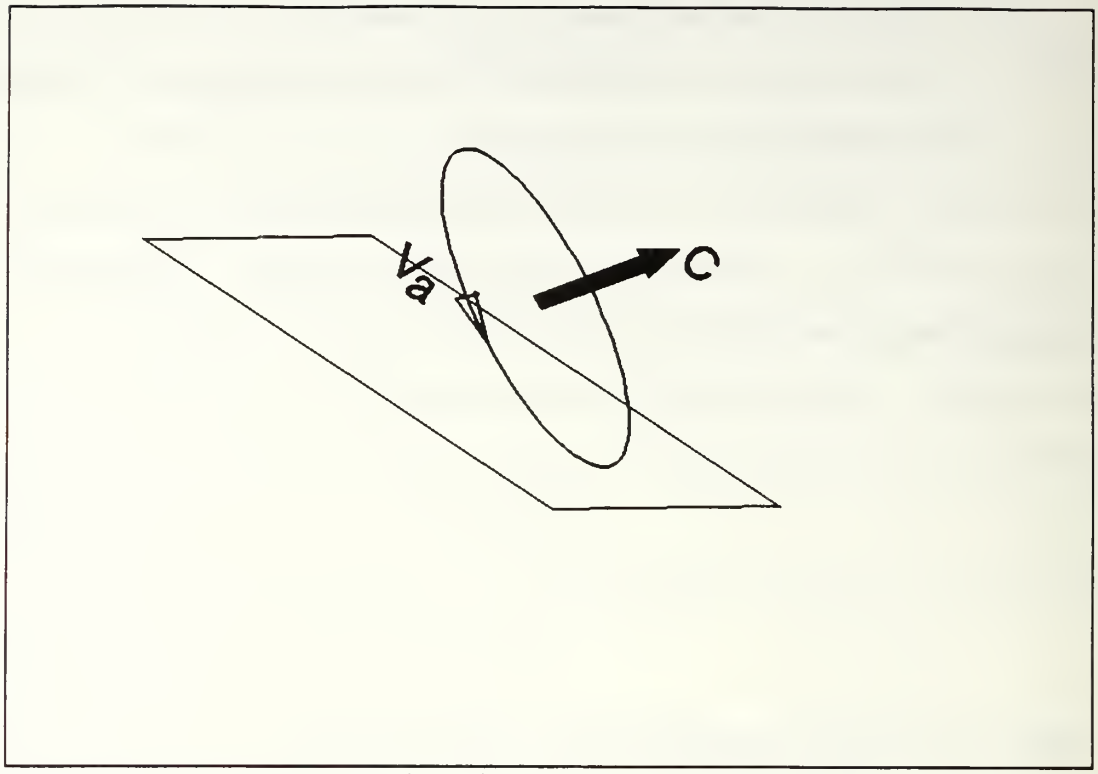

Figure 7. Ageostrophic circulation induced by C-Vector in three-dimensional space.

$$-\vec{k}\cdot\nabla\times(equation\ 26) \Rightarrow$$

$$\nabla^2 w_a = -2R_0\vec{k}\cdot\nabla\times\vec{C} \qquad (28)$$

Equation (28) demonstrates that the vertical velocity (w_a) is caused by the vertical vorticity of C-Vector (Figure 8).

Define:

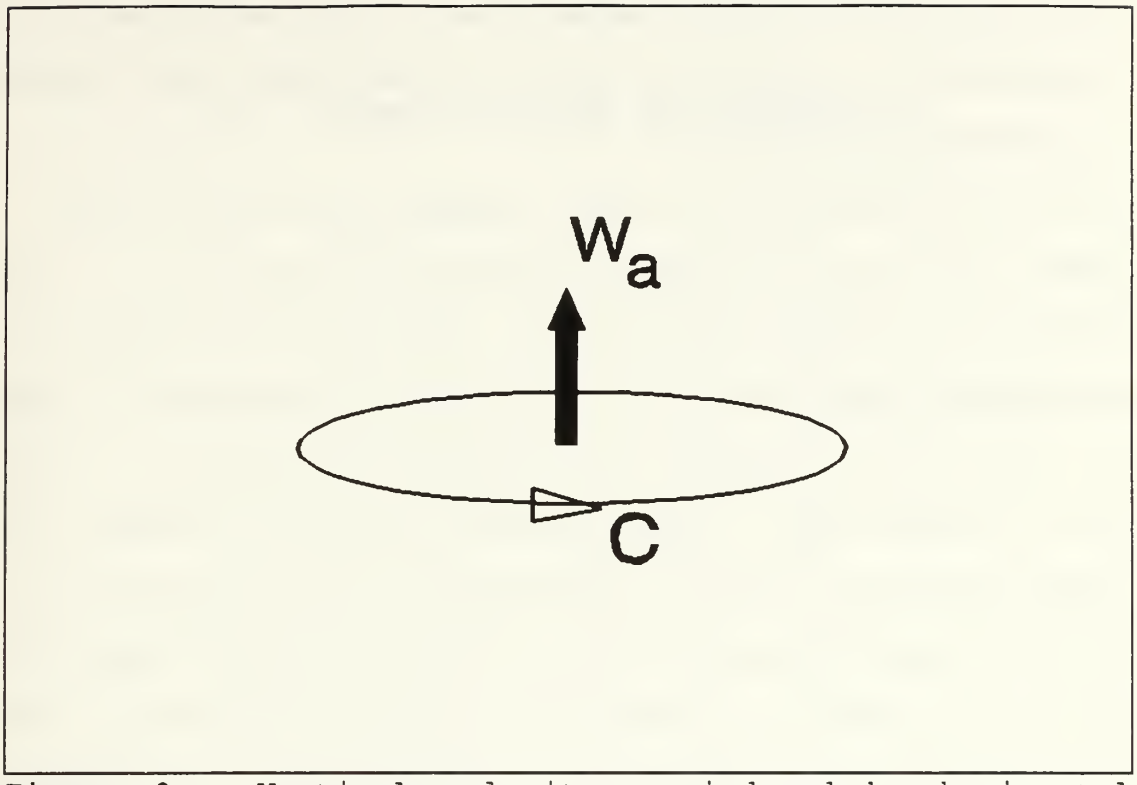

Figure 8. Vertical velocity w_a induced by horizontal rotation(vorticity) of C-Vector.

$$\Psi \equiv 2\left(\frac{\partial C_y}{\partial x} - \frac{\partial C_x}{\partial y}\right) \tag{29}$$

Combining equation (29) with equation (28) results in the following:

$$\nabla^2 w_a = -R_0 \Psi \tag{30}$$

Equation (30) is the Poisson equation. If normal mode solutions are considered, the vertical velocity w_a has the same sign as Ψ, therefore Ψ will be very useful because its positive (negative) values show positive (negative)

vertical ageostrophic velocities. The solutions provide information regarding upward (upwelling) and downward (downwelling) motion.

III. DATA COLLECTION AND PROCESSING

The *R/V Point Sur* departed from the Moss Landing Harbor on May 16, 1991 with a combined scientific crew from Naval Postgraduate School (NPS), Moss Landing Marine Laboratory (MLML), Scientific Applications International Corporation (SAIC), California Academy of Science (CAS) and the Environmental Protection Agency (EPA). The purpose of the cruise was to study oceanographic currents and hydrographic conditions in the area of the Gulf of the Farallones National Marine Sanctuary. The ship proceeded as planned along five across-shore transactions 20 km apart beginning with CTD station 1 (Figure 3). A total of 50 CTD casts were conducted to within approximately 25 m of the bottom. A brief ADCP survey was conducted as well (Figure 6).

This data was used to determine the pseudo-vorticity circulation of the region using the C-Vector concept.

A. DATA COLLECTION

1. CTD

All CTD stations with their positions, weather conditions and maximum depth (m) are shown in Table II. Stations 1, 20, 21, and 40 were not included because they were located outside the grid (Figure 9) which was used for the

Table II.CTD STATION LOCATION,WEATHER AND MAX.DEPTH

Stat. No.	Lat. Deg. N	Lat. Min. N	Lon. Deg. W	Lon. Min. W	Wind Dir.	Wind (m/s)	Air Temp. (C)	Max. Depth (m)
10	37	5.9	123	18.1	288	7.1	11.6	2858
9	37	10.2	123	8.8	289	11.7	11.3	1440
8	37	14.2	123	0.9	291	12.4	11.3	594
7	37	16.3	122	56.4	276	11.5	11.2	390
6	37	10.8	122	49.1	289	12.3	10.7	210
5	37	10.8	122	49.1	288	8.8	10.3	110
4	37	21.1	122	46.4	356	8.8	10.2	86
3	37	23.8	122	40.7	289	7.7	10.2	86
2	37	25.1	122	36.2	285	10.8	10.3	52
19	37	36.2	122	42.0	301	17.2	10.0	42
18	37	38.4	122	47.4	307	15.3	10.0	66
17	37	30.6	122	53.0	297	14.6	9.8	92
16	37	29.2	122	55.9	289	16.7	9.8	126
15	37	27.9	122	59.1	306	15.4	9.9	342
14	37	25.1	123	3.4	295	15.5	10.0	594
13	37	23.7	123	7.1	303	13.9	10.0	806
12	37	19.3	123	10.8	303	13.9	10.0	1400
11	37	15.5	123	25.0	316	11.7	10.0	2738
30	37	24.6	123	32.5	301	11.3	10.0	2840
49	37	29.0	123	23.4	305	12.0	10.3	2228
28	37	33.2	123	14.8	303	10.8	9.8	1630
27	37	35.4	123	10.8	297	8.8	9.8	1214
26	37	37.3	123	6.4	313	7.7	9.8	714
25	37	38.6	123	3.4	289	4.4	10.0	112
24	37	40.8	123	0.5	289	4.8	10.0	86
23	37	42.9	122	54.8	286	5.7	10.1	86
22	37	45.5	122	49.1	286	6.7	10.1	46
39	37	53.8	122	53.8	289	7.2	10.0	86
38	37	50.9	123	8.8	289	6.7	10.0	76
47	37	48.0	123	8.8	293	7.2	9.8	86
36	37	46.7	123	9.2	293	7.4	9.8	86
35	37	45.3	123	12.0	294	6.4	9.8	366
34	37	43.3	123	10.8	297	6.4	10.0	1054
33	37	41.0	123	20.8	292	8.8	10.0	1674
32	37	38.4	123	26.6	295	7.7	10.2	2712
31	37	34.9	123	34.9	313	6.4	10.7	3050
49	37	41.5	123	40.8	305	8.8	10.0	3146
48	37	45.6	123	32.2	289	7.0	10.5	2412
47	37	47.5	123	27.6	299	8.8	10.7	1620
46	37	49.5	123	23.3	298	7.3	10.5	582
45	37	50.9	123	20.2	299	3.8	10.6	112
44	37	52.3	123	17.5	289	4.0	10.7	98
43	37	55.0	123	11.7	288	7.2	10.7	90
42	37	57.8	123	6.0	275	6.2	10.5	74
41	37	59.1	123	3.2	270	4.7	10.5	40

calculation of the C-Vector. The CTD casts were made with a Neil Brown Mark III-B CTD attached to a General Oceanic rosette sampler for in situ water sampling. This model CTD is considered to be accurate to within ± 0.005 mmho, ± 0.005^0 C, and ± 6.5 db. Conductivity, temperature and pressure resolutions are 0.001 mmho, 0.0005^0 C and 0.1 db respectively.

The CTD sensors were calibrated prior to the cruise. Coefficients calculated for these calibrations were applied to the raw data. Salinities were further calibrated by adjusting the calculated salinity to the salinity of water samples collected during the cruise. Further details of instrument calibrations can be found in the NPS data report for this cruise (Jessen *et al.*, 1992).

2. ADCP

Continuous relative current velocity data was gathered aboard the *R/V Point Sur* using RD Instruments Vessel Mounted Acoustic Doppler Current Profile (VM-ADCP), equipped with a four beam JANUS array, operating at a frequency of 150 khz.

3. Wind data

During the cruise, an R. M. Young anemometer on the *R/V Point Sur* obtained 30 second averages of wind speed and direction (Table II).

4. Satellite

The AVHRR Instrument on NOAA-11 satellite measured emitted radiation of the study area in five wavelength bands

(three thermal Infra Red (IR) Bands, one Near Infra Red (NIR) and one Visible Band).

B. DATA PROCESSING

1. CTD

The raw CTD data was processed on a PC using an EG&G Marine Instrument software package called CTDPOST. This program flags bad data values using a first difference criterion and allows the user to examine and interpolate across bad data if necessary. After the correction of the data, a dual time lag filter was applied to remove time lag spikes, and the data was averaged to 2 db.

2. ADCP

The conversion of recorded ADCP relative velocity data into absolute velocity data took place on board ship. This process depends significantly on the accuracy of the ship's navigation instruments. The ship's position data was obtained from GPS and was also recorded on computer disks for later processing.

Variability of the ship's speed, direction, and data collection interval, play significant roles in the ADCP accuracy and reliability. More details concerning ADCP data processing techniques can be found in Kosro (1985). According to Kosro, accuracies of 4 - 5 cm/sec in the athwartship

component and 2 - 4 cm/sec in the fore-aft component are to be expected.

3. Wind data

The wind data, collected underway, was stored on the hard disk of an HP310 computer. This data was transferred to 5.25 inch diskettes upon return to port and computer processed to obtain hourly averaged wind vectors (Figure 4).

4. Satellite data

The Satellite data was first calibrated, transferred to earth coordinates and temperature calculated pixel by pixel. All images were coregistered to a similar coordinate map of the study area. This work took place at the Naval Postgraduate School IDEA Lab.

5. Geostrophic velocities

All densities and geostrophic velocities were obtained from the calibrated CTD data using computer programs developed in the NPS oceanography department based on the equation of state of seawater (Fofonoff, 1985).

The u and v components are the across shore and along shore components of the geostrophic velocities. These components at a particular station were calculated using stations on either side of it. For example, utilizing stations 26 and 24, the v-component of geostrophic velocity of station 25 can be determined, and from stations 16 and 36, the u-component of station 25 (Figure 9).

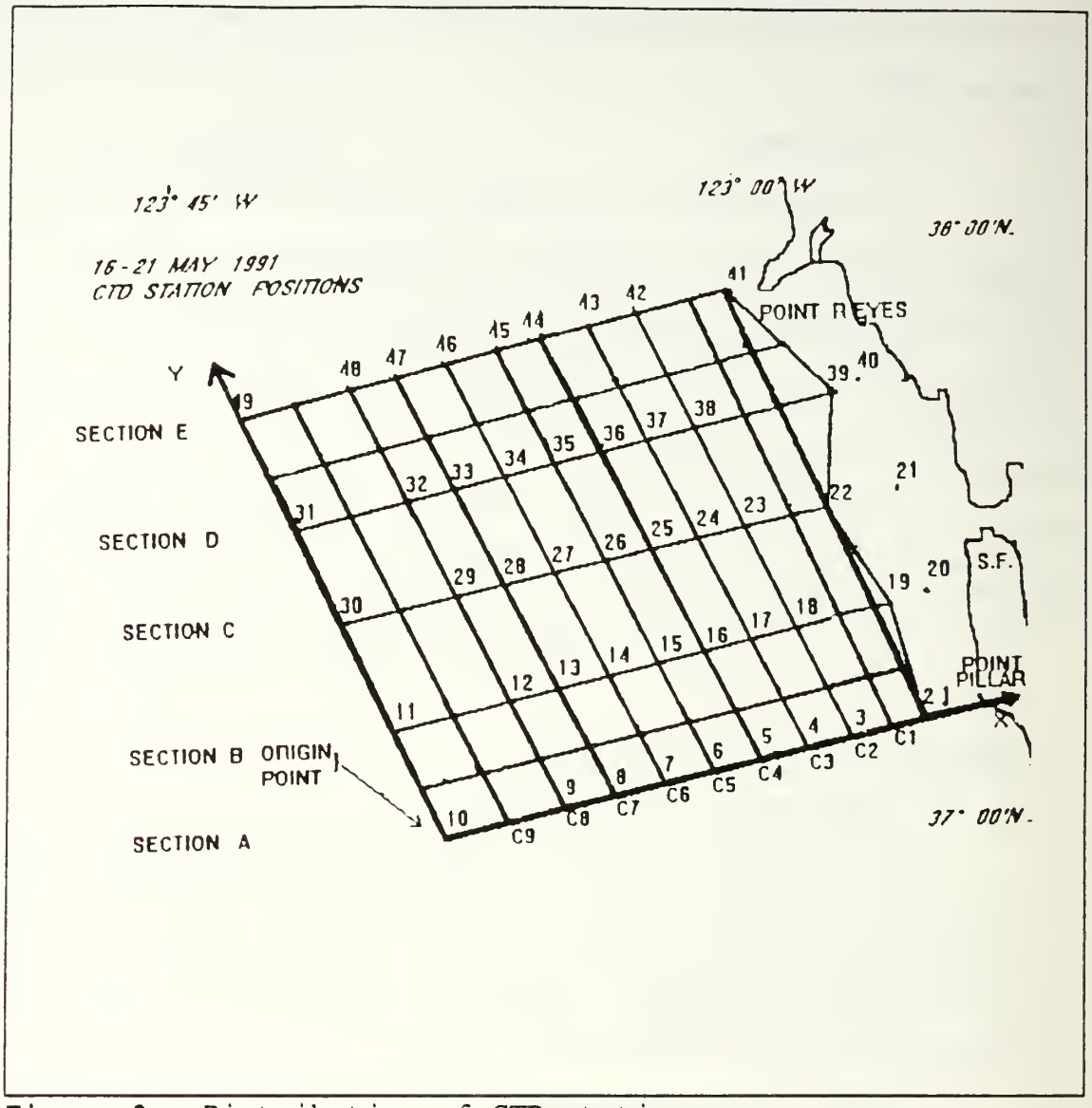

Figure 9. Distribution of CTD stations.

This does not work for the external stations. In this case the u and v components of the external stations were calculated using the external stations and the stations close to them. For example, for the determination of the u-component of geostrophic velocity at station 3, stations 3 and 18 were used.

6. Reference level or Level of No Motion (LNM)

The calculation of geostrophic velocities depends on the right choice of a reference level or Level of No Motion (LNM).

The hydrographic and ADCP data from the NPS Farallones Shelf and Slope study on May 16 to May 21, 1992 were examined carefully. It was determined from the plots of the vertical sections of 5 km averaged, across and along-transect ADCP velocities (for sections A, B, C, D and E) that the existence of a common horizontal reference level or LNM was uncertain. It was obvious that the reference level could not be horizontal over a great distance.

In this study a large number of stations were located in shallow waters so the area was divided into two parts (Figure 10). A shallow part which includes stations with depths less than 1,000 meters (over the continental shelf), and the deep part which includes stations with depths more than 1,000 meters (over the continental slope). It was assumed that the reference surface was horizontal within the deep waters.

According to Soule (1939) the water density field has to be analyzed first and the horizontal reference surface has to be placed in the layer where density is least disturbed.

In analyzing the distribution of density differences between neighboring stations the depths were found where

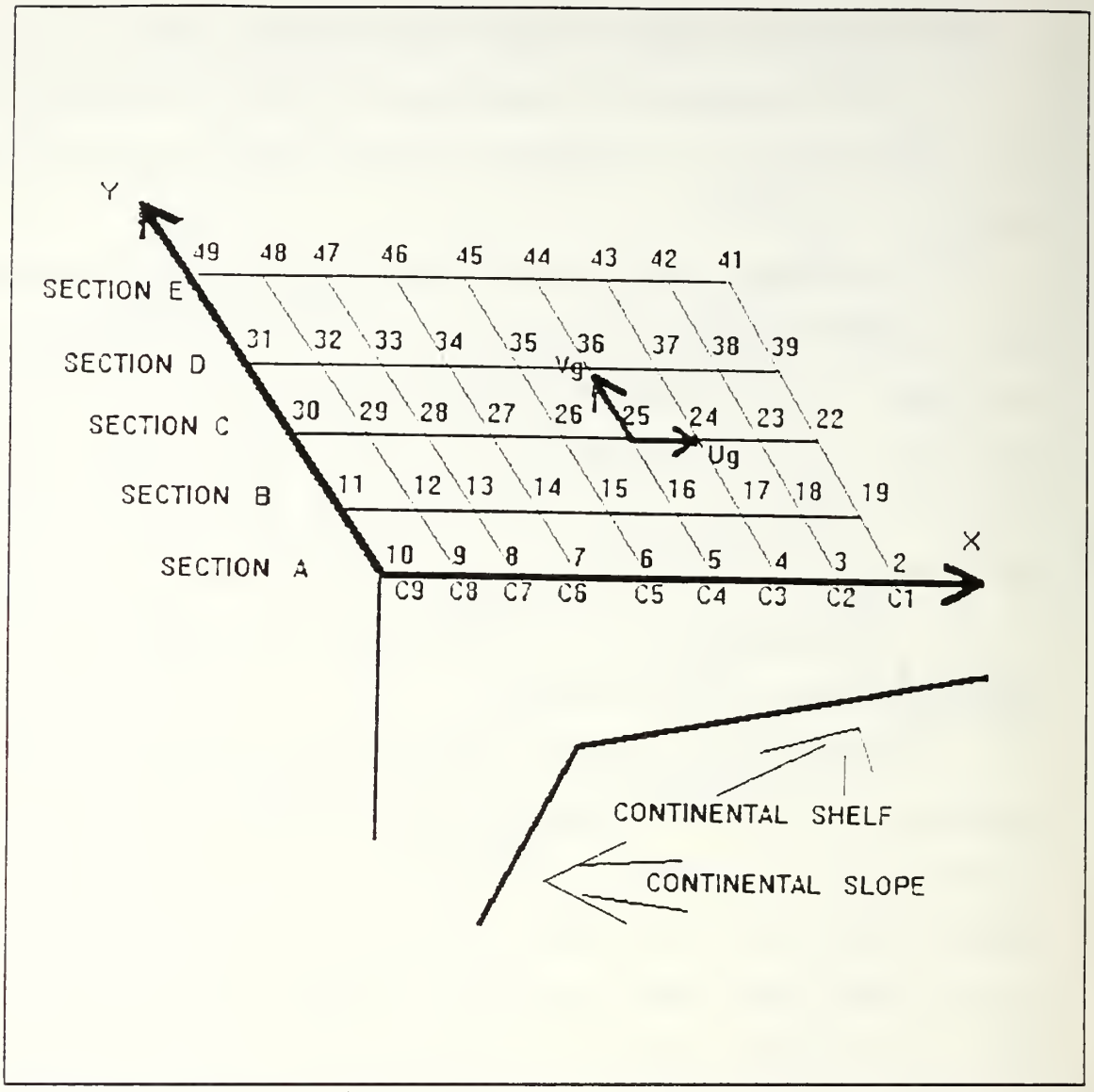

Figure 10. A 3-D view of the stations over the shallow and deep waters.

density differences changes sign or became zero. These depths represent the levels of minimum current shear.

Figure 11, which illustrates the plots of the density differences between neighboring stations in the shallow part of Section D, shows that there is no common depth where the

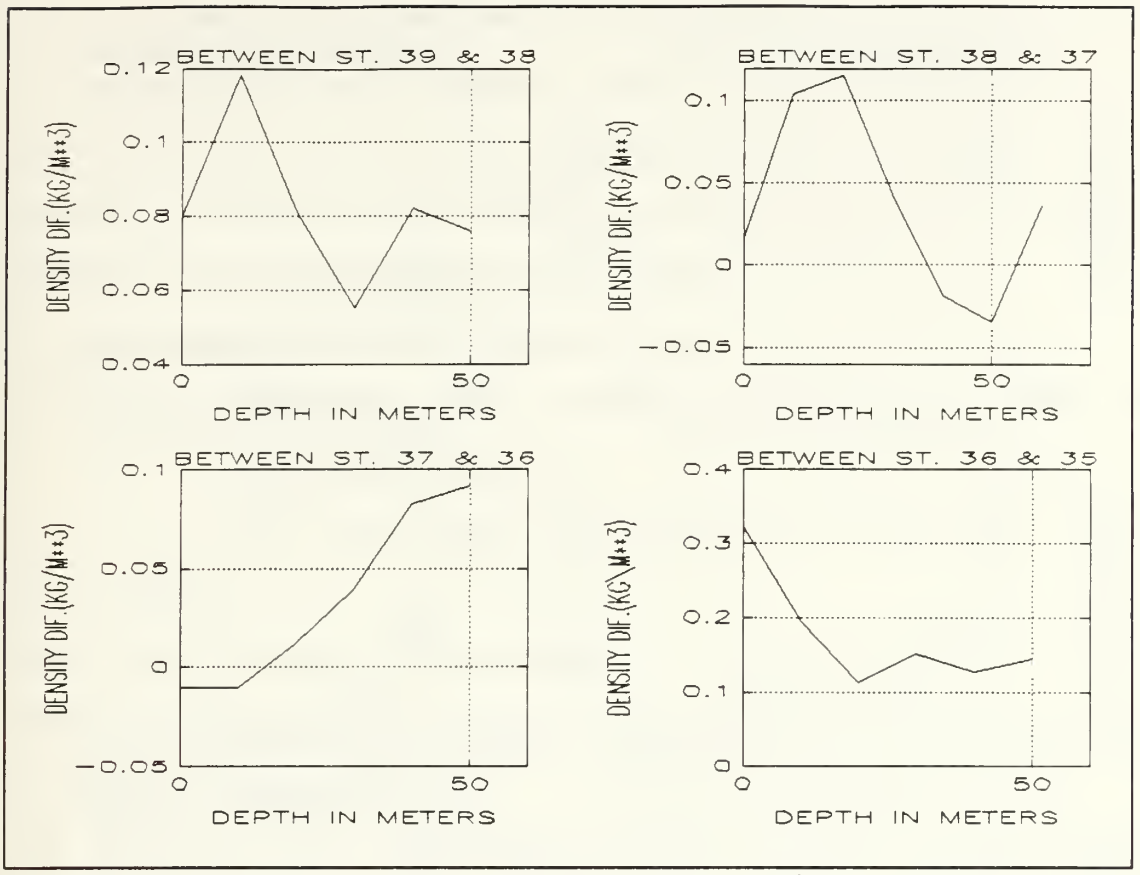

Figure 11. Density differences between pairs of stations of Section D.

density differences are zero. The choice of the LNM in shallow waters is therefore uncertain, and the reference layer was estimated to be the lower level of measurements between neighboring stations.

The analysis of density difference distribution for deep stations offers better results. Figure 12 includes all the pairs of deep stations. A common depth of "zero" density differences is found at 1,400 meters. This level (1,400 m) was used as a reference level for deep waters.

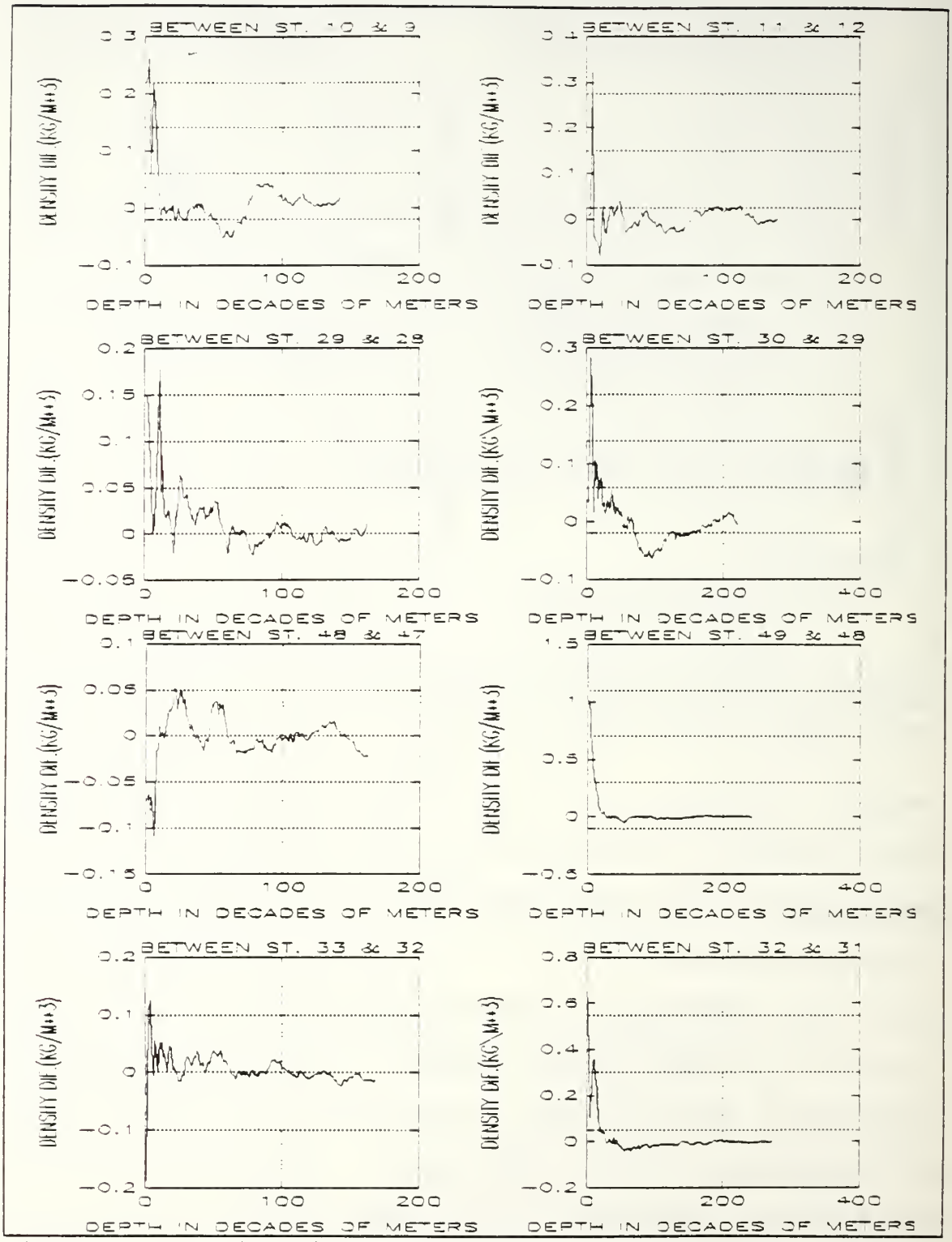

Figure 12. Density differences between pairs of deep stations.

There is another method of determining the LNM similar to the above process (Mamaev, 1955). The difference is that the curves for the vertical distribution of differences of specific volume at two neighboring stations are analyzed, instead of the differences of density.

7. Computation of C-vector

a. Calculation of C-vector (C_1, C_2, C_3) from the geostrophic currents.

The computation was done using equations (16) - (18), where:

- U_g and V_g can be calculated for all stations.
- Coriolis parameter was assumed constant, $f=2\Omega\cos\phi$ (where Ω = 7.29 10^{-5} sec^{-1} and an average latitude ϕ = 37^0 30′ North is used)
- Y^y and Y^x, the turbulent momentum fluxes due to surface wind stress (τ^x, τ^y), are given by equations (6)

Taking the average density of all stations it was determined that an average ocean density of the region was ρ_0= 1.026 gr/cm^3.

Wind stress (τ^x, τ^y) is obtained from :

$$\tau^x=\rho_a C_D|\vec{V}_w|u_w \quad , \quad \tau^y=\rho_a C_D|\vec{V}_w|v_w \qquad (31)$$

where ρ_a = 1.293 10^{-3} gr/cm^3 (air density), C_D = 1.3 10^{-3} (drag coefficient), $|V_w|$ is the hourly averaged wind speed at

height 10 m and u_w, v_w are the x and y - components of wind speed respectively.

The mixed layer depth (MLD) of the study area is needed to determine to what depth the wind mixing influences the ocean stratification. Observing all MLD from temperature plots during this study, it was determined that an average MLD (of all stations) is 15 m. This means that wind stress mixes the waters down to 15 m.

A linear reduction of wind stress with respect to z was assumed (Figure 13) for the purposes of C-Vector calculation.

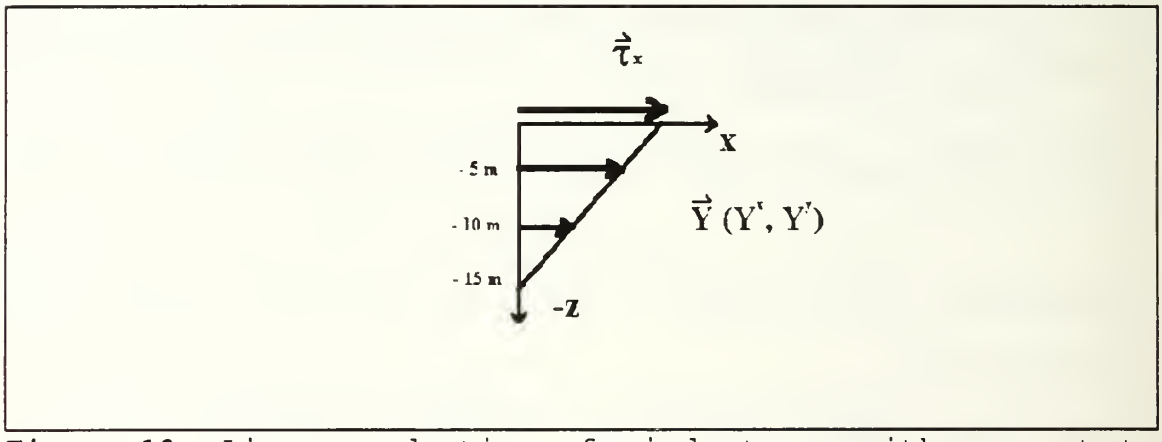

Figure 13. Linear reduction of wind stress with respect to depth.

b. Computation of C-vector (C_x, C_y, C_z) due to the total flow (geostrophic and ageostrophic).

This computation depends on the equations (22) - (24) where C_1, C_2 and C_3 and geostrophic velocities are calculated as described above.

Having C_x, and C_y it is then easy to compute Ψ from equation (29). Contours of C-Vector for ageostrophic flow, C-Vector for the total flow and Ψ are analyzed and compared in the next chapter. These three parameters are the main tools for the identification of the ageostrophic and the total (geostrophic and ageostrophic) pseudo-vorticity fields.

IV ANALYSIS OF PSEUDO-VORTICITY FIELDS

A. DESCRIPTION OF THE ANALYSIS

This chapter presents a detailed description of the pseudo-vorticity fields for the ageostrophic circulation (C_1, C_2, C_3) in the Gulf of the Farallones. The results of this description enable us to proceed further in the analysis of the pseudo-vorticity fields for the total geostrophic and ageostrophic circulation (C_x, C_y, C_z). Then the vorticity of C-Vector (Ψ) will be used to indicate the upward and downward motions in the area, and it will be compared to a satellite picture of the same area and the vertical ADCP velocities.

1. Pseudo-vorticity fields (C_1, C_2, C_3) for the ageostrophic circulation

a. Analysis of the x-component of ageostrophic pseudo-vorticity field

C_1 is the ageostrophic pseudo-vorticity component of C-Vector in the x-direction or cross-shelf direction. This direction approximately indicates the cross polar vertical circulation pattern. The values for C_1/f^3 have been plotted on the y-direction or along-shore direction.

From Figure 9, notice that there are nine columns on the y-direction. Columns 1, 2, 3, 4 and 5 correspond to shallow water and are going to be analyzed first.

Figures 14, 15 and 16 show the plots of the first five columns. The arrows on the plots indicate the direction of rotation of the ageostrophic pseudo-vorticities and not the directions of currents. The cells with positive (negative) values of the ageostrophic pseudo-vorticity are turning counter-clockwise (clockwise) or cyclonic (anti-cyclonic). The direction along the positive (negative) axis is upward (downward) out of the page (into the page).

From these five plots it can seen that the ageostrophic pseudo-vorticities are increasing going offshore. At column 1, the maximum values of C_1/f^3 are about +/- 0.1 and at column 5 the values have increased to 1.3. The first two columns have the negative ageostrophic pseudo-vorticity cells north and the positive cells south. The opposite occurs at columns 3 and 4 and at column 5 the positive ageostrophic pseudo-vorticity predominates from South to North.

At column 5 the strong south positive ageostrophic pseudo-vorticity cell coincides with the area of large temperature and salinity gradients of Section A (Figure 6). Also, the strong middle positive ageostrophic pseudo-vorticity cell coincides with the significant salinity gradient of Section D (Figure 6). Column 5 has the largest positive value of the ageostrophic pseudo-vorticity fields.

Figures 16, 17 and 18 show the four plots of columns 6, 7, 8 and 9 which lay over the deep waters. Column

7 shows a strong positive ageostrophic pseudo-vorticity field that dominates the area. Columns 6 and 8 have their negative ageostrophic pseudo-vorticity cells on the north side and Column 6 has one positive cell south. Column 8, however, has a positive cell followed by another negative cell south of the north positive cell. Column 9 has a significant negative north ageostrophic pseudo-vorticity field. Its position coincides with the large temperature and salinity gradient of the west side of Section E (Figure 6).

The significant temperature and salinity gradients are probably due to subarctic water underlying a surface lens of fresh and warm water (Collins, 1992). Figure 19 presents a better picture of the ageostrophic pseudo-vorticity fields through a 3-D plot of columns 9,7 and 5. The red lines are the solid positive values and the blue lines are the dashed negative values.

The majority of the ageostrophic pseudo-vorticity fields are located at the upper 200 m. Waters below 200 m were found to have very weak ageostrophic circulation, so the significant ageostrophic circulation is close to the surface.

b. Analysis of the y-component of the ageostrophic pseudo-vorticity fields

The values for C_2/f^3 have been plotted at the five Sections A, B, C, D, and E (Figures 20, 21 and 22). Section A shows a relatively weak ageostrophic pseudo-vorticity field.

The plots of Sections B and C include four cells. Moving off shore alternating values of negative and positive cells are observed. Sections D and E have the highest values of the non-dimensional component C_2/f^3. The west (left) side of Section E has the maximum negative value of the ageostrophic pseudo-vorticity fields. This location coincides with the large off - shore temperature and salinity gradient of section E (Figure 6). The values of C_2/f^3 below 200 m are very small as can be seen from the plot of Section C (Figure 21).

The magnitudes of C_2/f^3 (maximum value -7) are larger than the magnitudes C_1/f^3 (maximum value 1.3). This probably happens because the average distance between the five sections (dy = 20 km) is bigger than the average distance between the nine columns (dx = 8 km), and the derivatives with respect to y are smaller than the derivatives with respect to x.

Figure 23 offers a three dimensional view of the ageostrophic pseudo-vorticity cells of Sections A, C and E. All the sections show that the ageostrophic circulation is located close to the surface and close to the locations of the large temperature and salinity gradients.

c. Analysis of the z-component of ageostrophic pseudo-vorticity field

As expected the values of vertical component C_3/f^3 are smaller than the values of the horizontal components

because the vertical ageostrophic vorticity is much smaller than the vertical geostrophic vorticity.

The upper plot of Figure 24 shows C_3/f^3 at the surface, without the wind affect. Notice that there are three negative ageostrophic pseudo-vorticity cells and one positive. The large values of C_3/f^3 are concentrated at the north-west side of the area where the large temperature and salinity gradients were observed before. The lower plot of Figure 24 shows the contours of C_3/f^3 including the wind. The majority of the values of C_3/f^3 are negative at surface. This probably happens because the area with the negative values coincide with the area of strong winds. A comparison of the plot of C_3/f^3 at the surface with wind and without wind shows that without wind there is one cell with relative large positive values of C_3/f^3 on the North-West side.

The plot which includes the wind shows that the negative values predominate in the region, and the positive cell that existed without the wind has become smaller and weaker (the magnitude is smaller). For C_3/f^3 at 50 m (Figure 25), the three negative cells and the one positive cell exist at the same positions but with smaller values.

At 200 m (Figure 25), the three negative cells still exist almost at the same location but with smaller magnitudes. The previously formed positive cell is very weak, and a new positive cell appears at the south-east corner of

the area. Figure 26 shows a three-dimensional picture of the three plots of C_3/f^3 at the surface and the depths of 50 m and 200 m.

Figure 27 shows a 3-D picture of C-Vectors of columns 9, 7 and 5. The large negative values of C-Vector (for ageostrophic circulation) were found at the west side of Section E where the large temperature and salinity gradients were observed.

2. Pseudo-vorticity fields for the total circulation (C_X,C_Y,C_Z) ageostrophic and geostrophic

a. Analysis of the x-component of C-Vector (C_x) of the pseudo-vorticity field

The columns 1, 2, 3, 4 and 5 are located over the shallow waters. At these columns the negative pseudo-vorticity fields are dominant (Figures 28, 29 and 30). The strongest cells are located south and north of column 5, and the south one coincides with the large temperature and salinity gradients at the middle of Section A.

At the deep waters, the negative cells of pseudo-vorticity are dominant also (Figures 30, 31 and 32). At the north part of column 8 and 9, the maximum values of C_x/f are observed (C_x/f = -35). In the same area, maximum values of C_1/f^3 and C_2/f^3 and C_3/f^3 were seen before. This is the area with maximum temperature and salinity gradients. The arrows show an upward flow at column 9. At column 8, there is an

upward motion south and north and at the middle downward flow. The arrows indicate the upward and downward motion of all columns.

Figure 34 is a three-dimensional plot of C_x/f for columns 9, 7 and 5 where the upward-downwards motion can be seen more clearly in three-dimensional space.

b. Analysis of the y-component of C-Vector (C_y) of the pseudo-vorticity field

Positive pseudo-vorticity cells of C_y dominate the five sections (Figures 34, 35 and 36). Notice that a negative pseudo-vorticity cell exists at the west side of all Sections. The arrows show an upward motion off shore of all Sections followed by a downward motion (going east). At Sections A, B, and C, there is an indication of upward motion at the east side of these sections. Sections D and E have the strongest pseudo-vorticity cells at their west side (maximum C_y/f = 13 at Section D). This area contains the large horizontal temperature and salinity gradients. Figure 37 contains a better picture (3-D) of the pseudo-vorticity fields of Sections A,C and E.

c. Plots of Ψ function

Figure 38 shows Ψ at the surface. The large positive values of Ψ mark an upward motion at the west side of the region. In the same figure, there is an outer area

west of the Farallones Islands where there are positive values of Ψ and these are probably upwelling waters.

Between these two areas, there is an area with negative values of Ψ (downward motion). This area lies over the continental slope. A weak upward motion (positive values of Ψ) appears at the east side of the region and south-east of Farallones Islands. At 20 m, the picture is similar to the surface.

At 50 m (Figure 39), the locations of upward and downward regions are almost the same as those seen at the surface and 20 m. At 200 m, the situation starts to invert, and the regions of upward motions become regions of downward motions. This means that the upward-downward motions do not extend as deep as 200 meters.

Figure 40 is a 3-D plot of Ψ at surface, 50 meters and 200 meters. In this color picture the solid positive values are red (upward motion) and the dash negative values are blue (downward motion).

B. VERIFICATION OF C-VECTOR VORTEX LINES

1. Direct verification of C-Vector vortex lines by Ψ function

An important verification of the upward and downward water motions at Gulf of Farallones Islands induced by C-Vector can be achieved by the Ψ function. The positive values

of Ψ give the upward motion (upwelling) and the negative values the downward motion (downwelling).

From examining the plots of Ψ, C_x and C_y it was determined that when C_x and C_y vortex lines indicate an upward (downward) motion, they were consistent with the positive (negative) Ψ lines.

2. Indirect verification of C-Vector vortex lines by SST images

Figure 41 is an AVHRR image of the area for the day prior to the cruise (15 May 1991). It suggests that a plume of cold water (8^0 C) extends offshore of Point Reyes and over the continental slope. This area coincides with positive values of Ψ (upward motions) south-west of Farallones Islands (Figure 38).

South-east of the continental slope and north-west of the Pioneer Seamount, there is an area of relatively warm water (10^0 - 11^0 C). At this area, Ψ has negative values (downward motion). At the south-west side of Pioneer Seamount, there are relatively cold waters (9^0 - 10^0) and at the same area, Ψ has positive values. Therefore, the SST images provide useful information concerning possible vertical velocity at the ocean surface and are a helpful indirect verification of Ψ.

3. Comparison of vertical ADCP velocities with Ψ function

Figures 42 and 43 shows the vertical ADCP velocities at 20 m and 50 m at the upper part of the figures, and Ψ at 20 m and 50 m at the lower part of these Figures. Notice that at 20 m depth and at the south-east of the region, both Ψ and vertical ADCP velocities are consistent because they show negative values. The Ψ has negative values at the center of the region, but the vertical ADCP velocities are negative at the south-west side of the area. These two regions of negative values coincide partially. The rest of the areas have positive values.

At the plots of 50 m, the vertical ADCP velocities indicate negative values at the same areas as at 20 m. The Ψ shows negative values at the east side of the region and at the middle and south region. The areas of negative values of Ψ and negative vertical ADCP velocities partially coincide and partially differ.

There is no perfect match. This happens probably because the vertical ADCP data are also affected by tides, waves or internal motions. Also, the calculation of Ψ contains some small errors like the round-off error, truncation error and machine error.

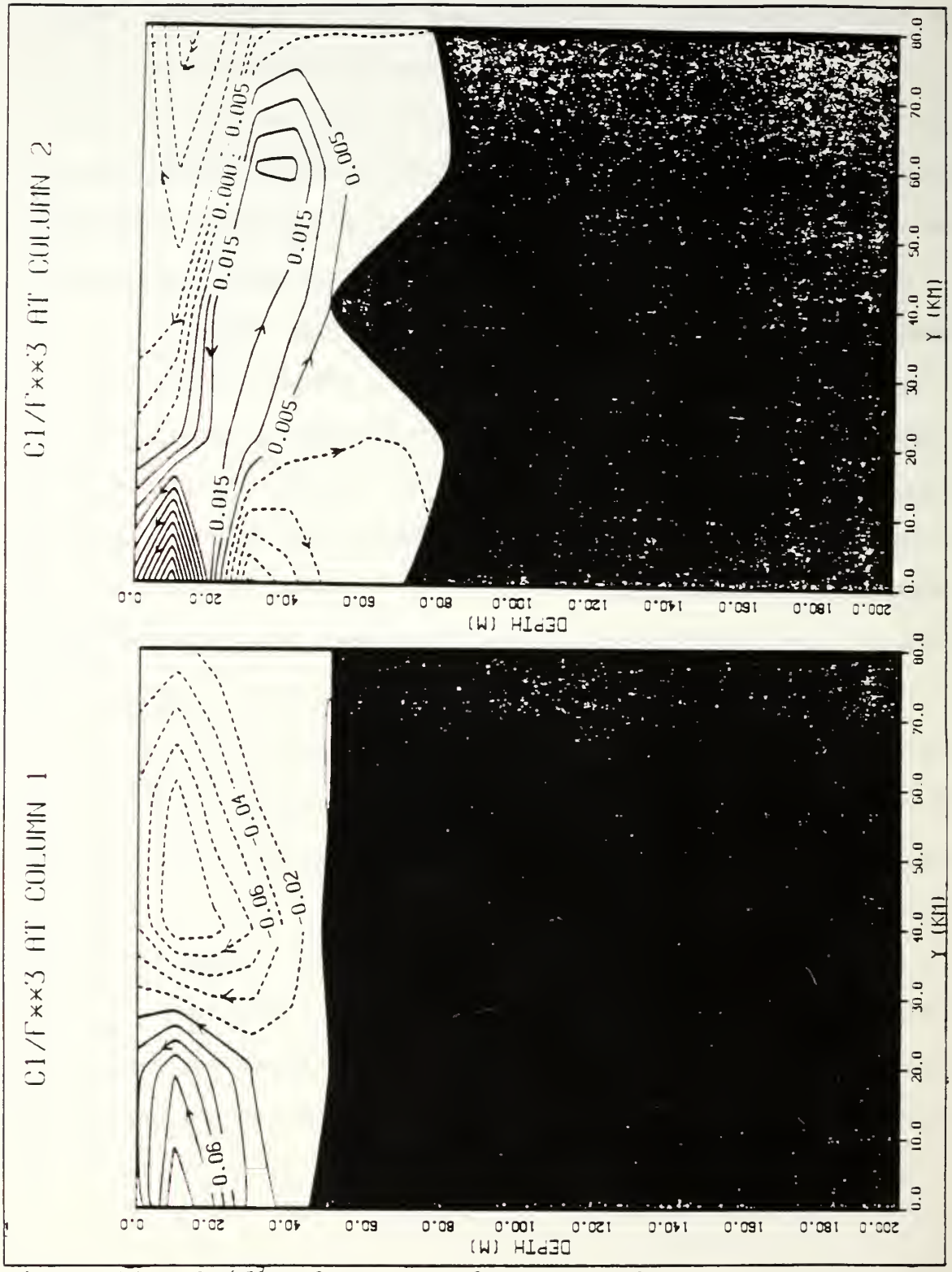

Figure 14. C_1/f^3 values at columns 1 and 2.

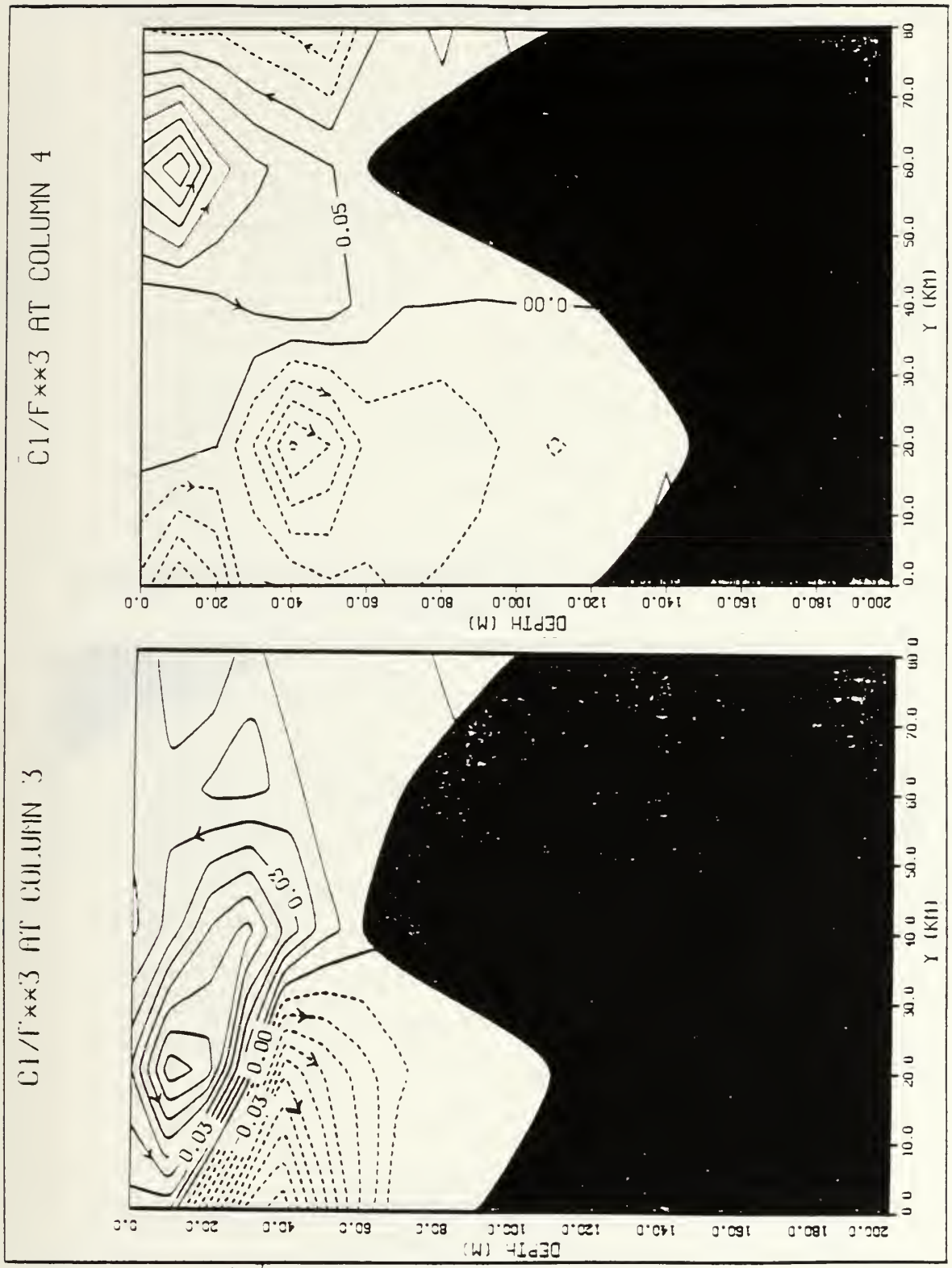

Figure 15. C_1/f^3 values at columns 3 and 4.

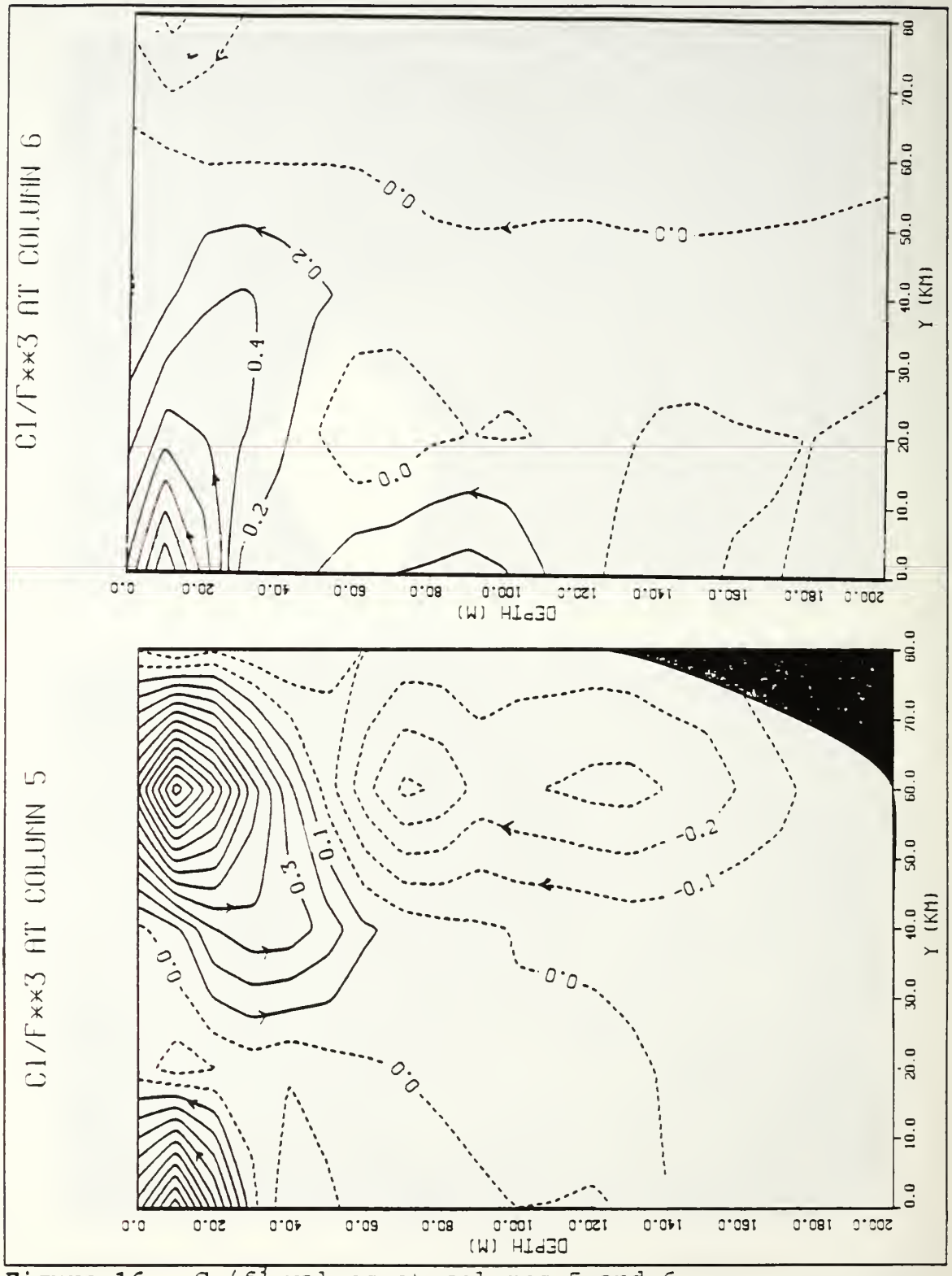

Figure 16. C_1/f^3 values at columns 5 and 6.

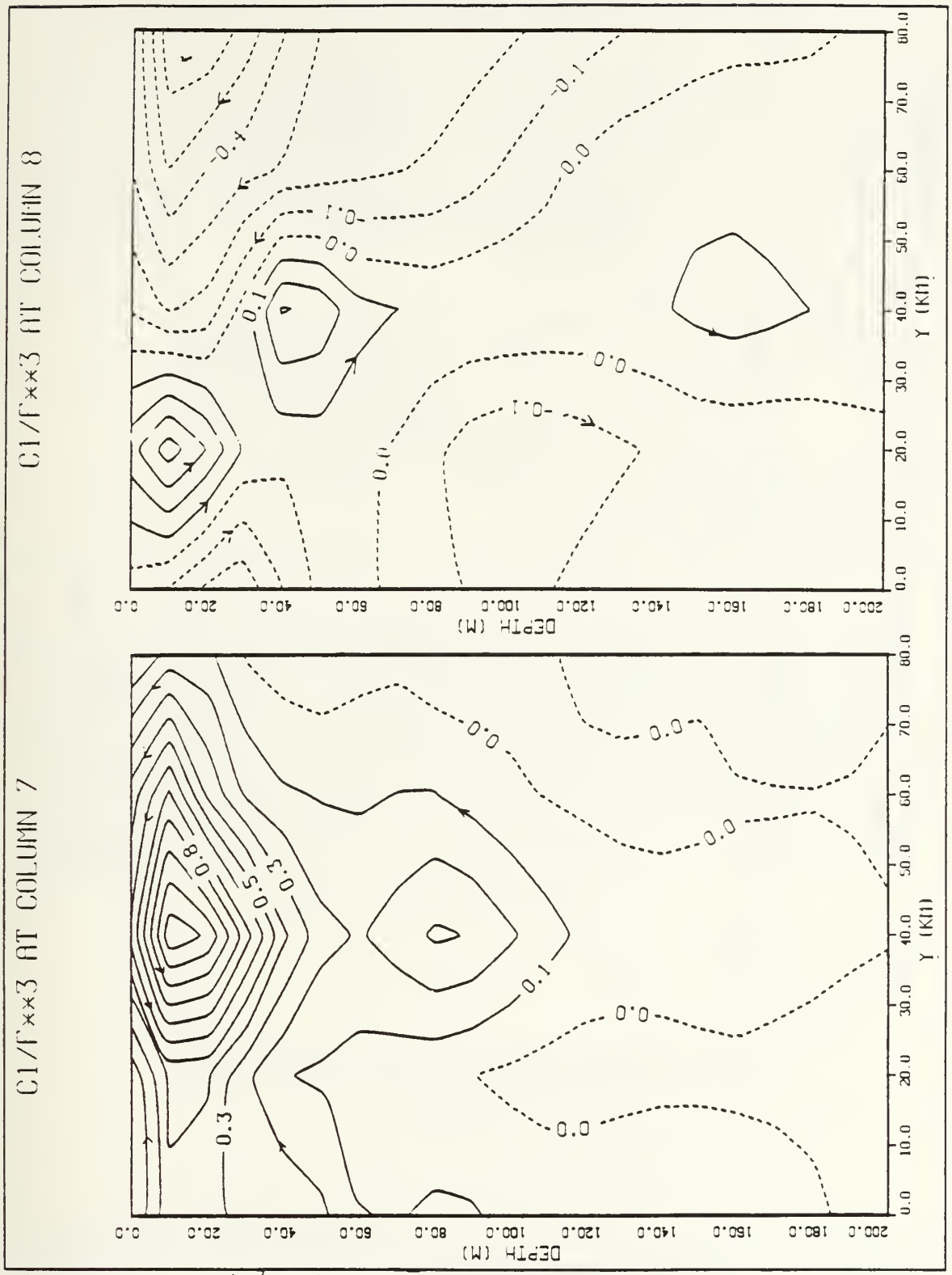

Figure 17. C_1/f^3 values at columns 7 and 8.

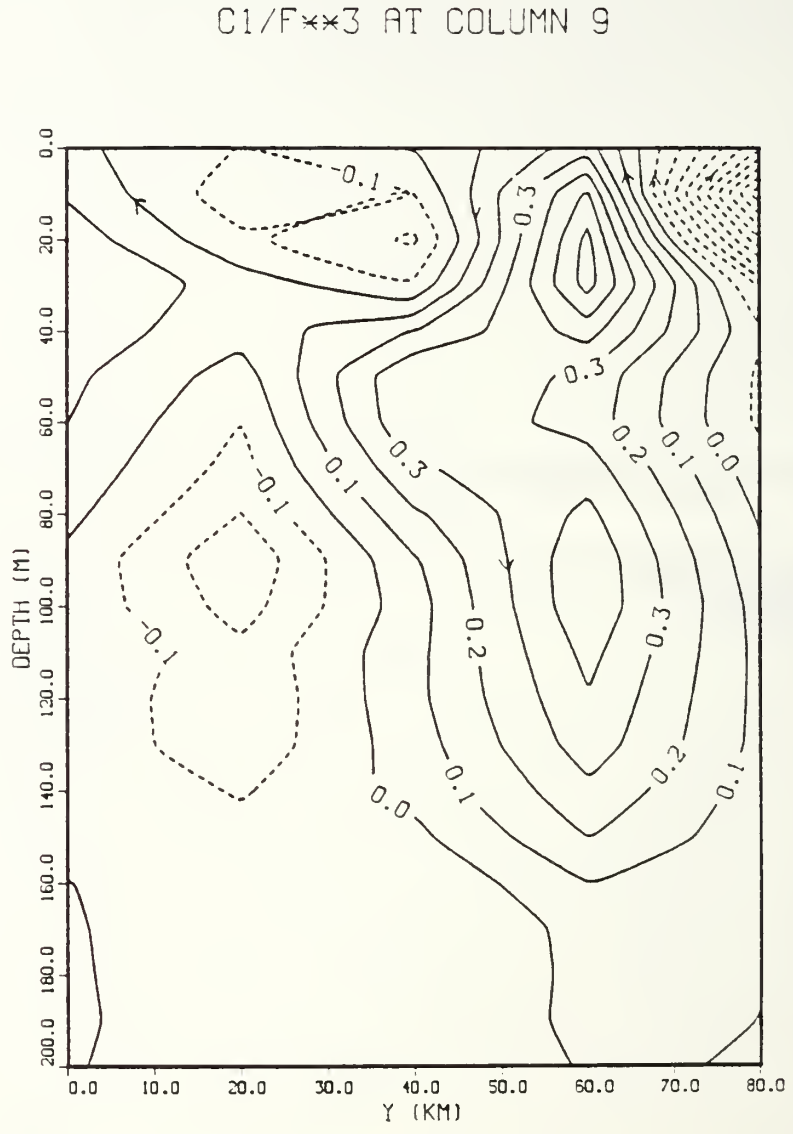

Figure 18. C_1/f^3 values at columns 9.

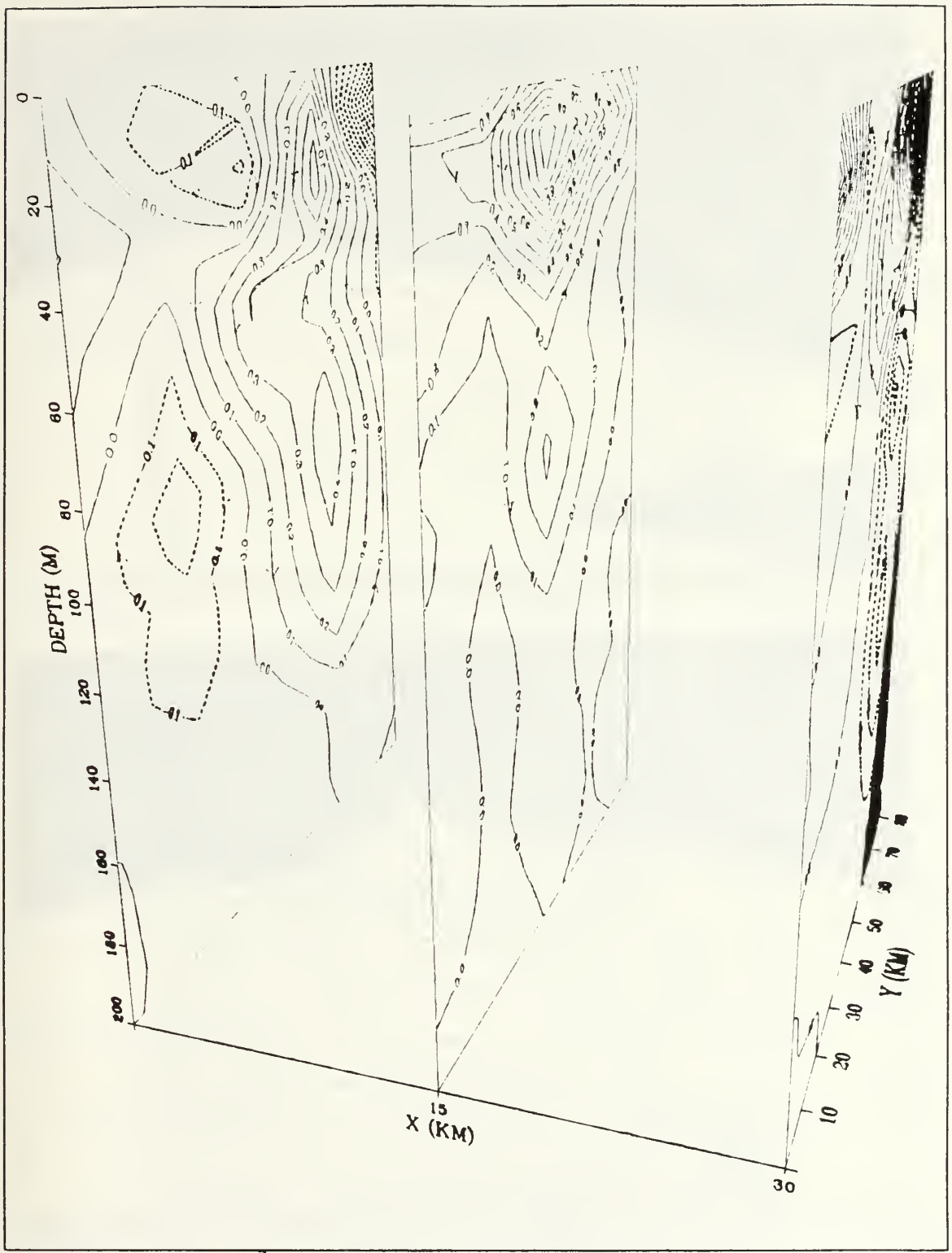

Figure 19. C_1/f^3 values at columns (from left to right) 9,8 and 7.

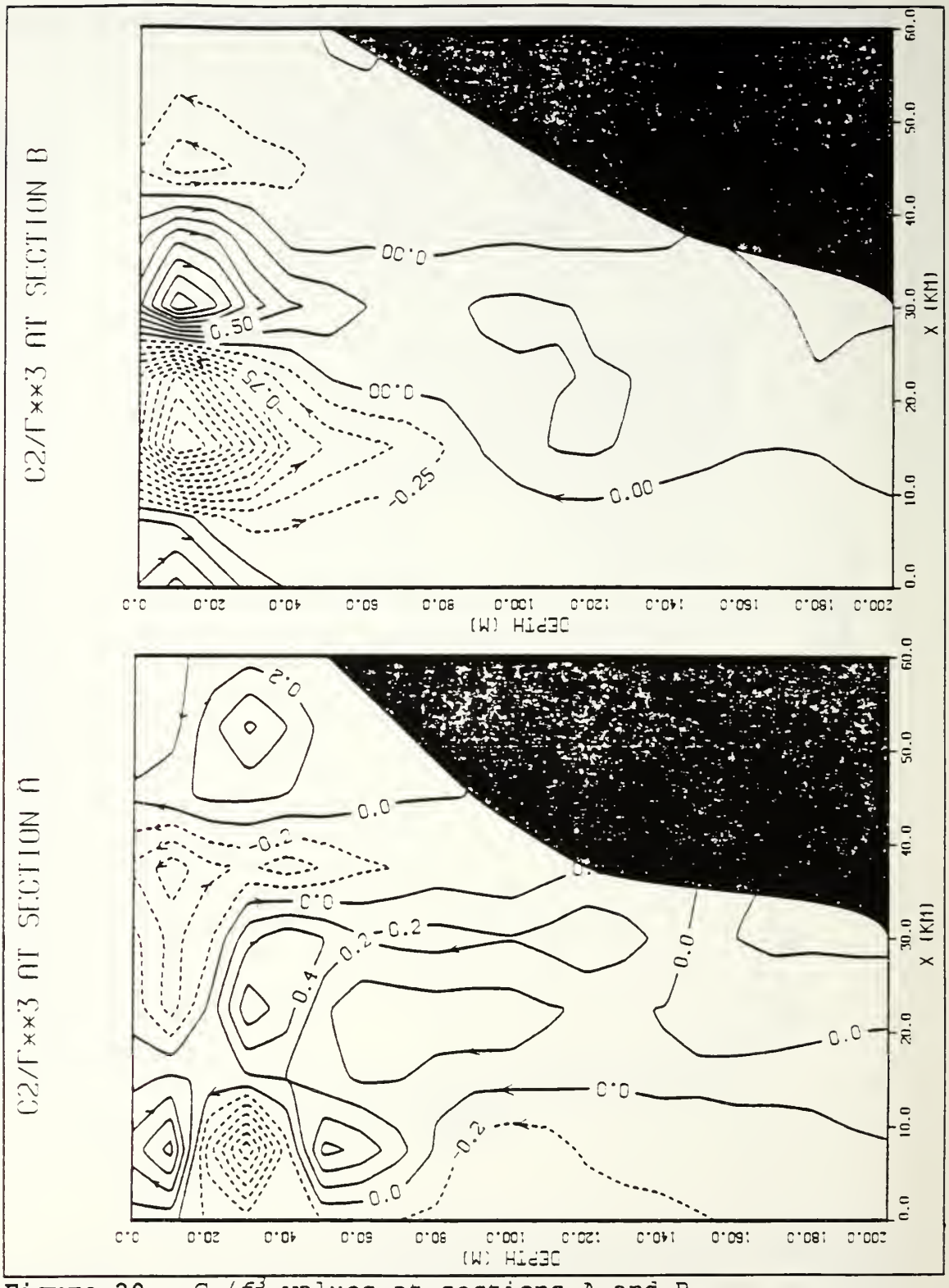

Figure 20. C_2/f^3 values at sections A and B.

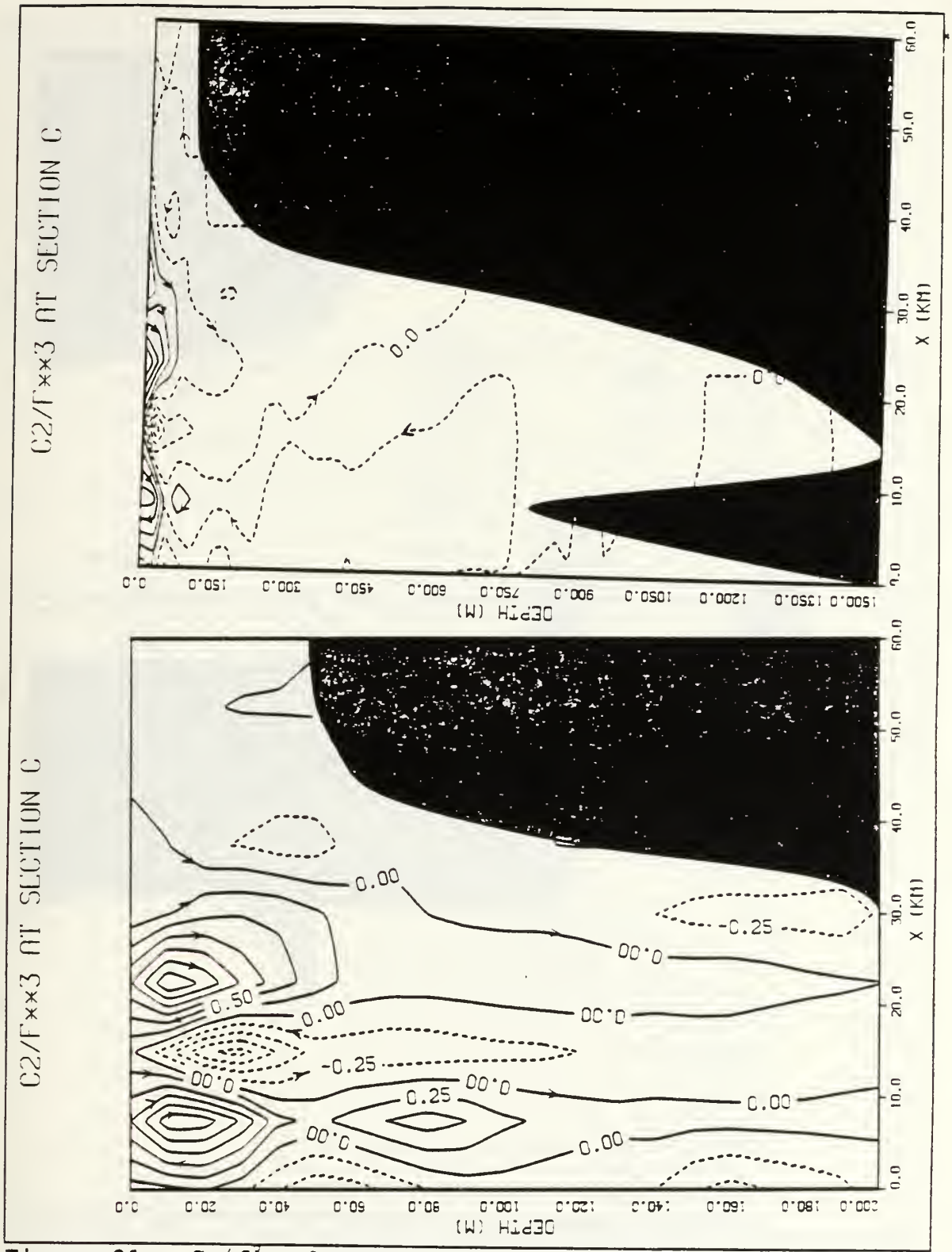

Figure 21. C_2/f^3 values at sections C and D.

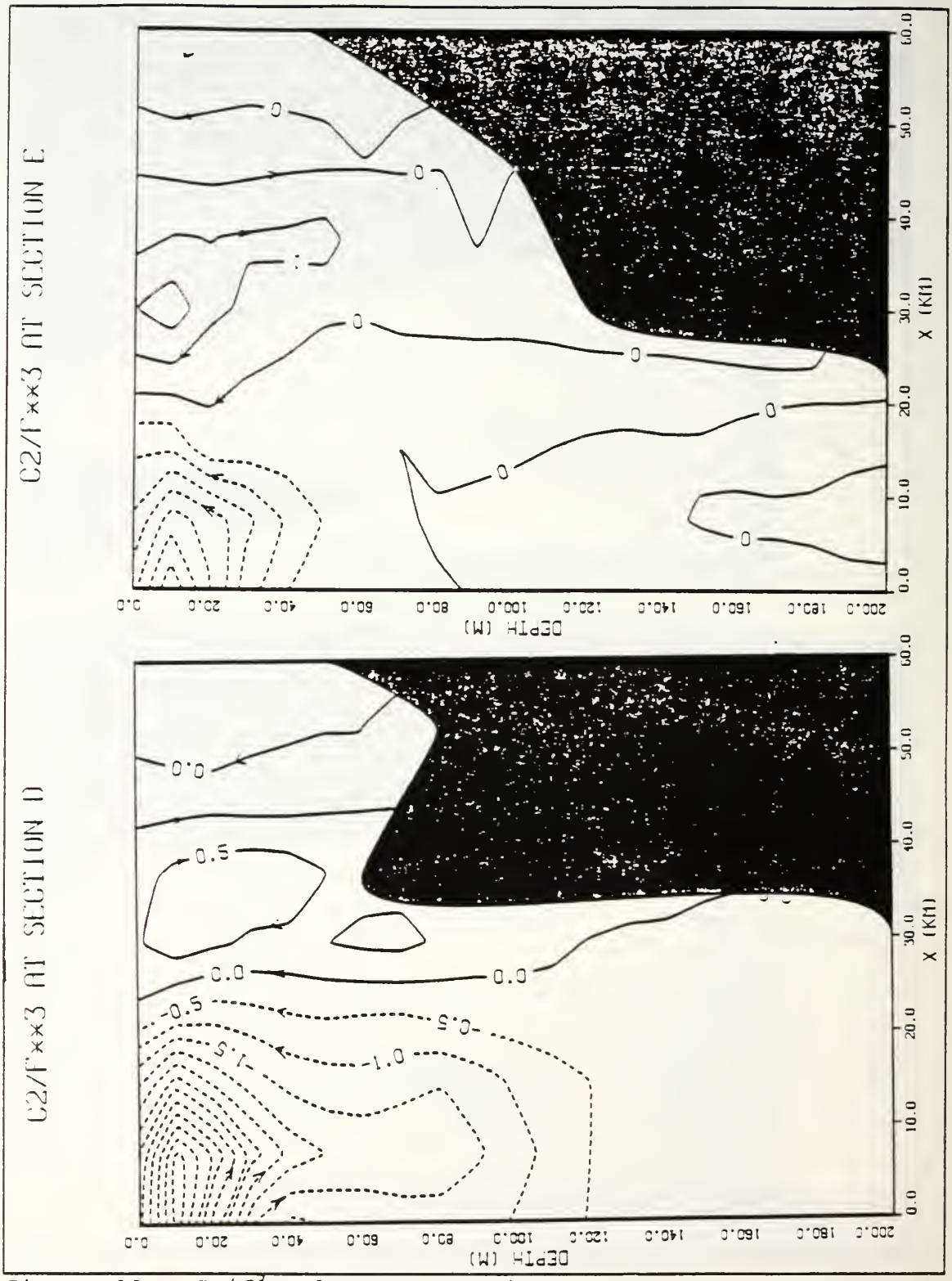

Figure 22. C_2/f^3 values at section E.

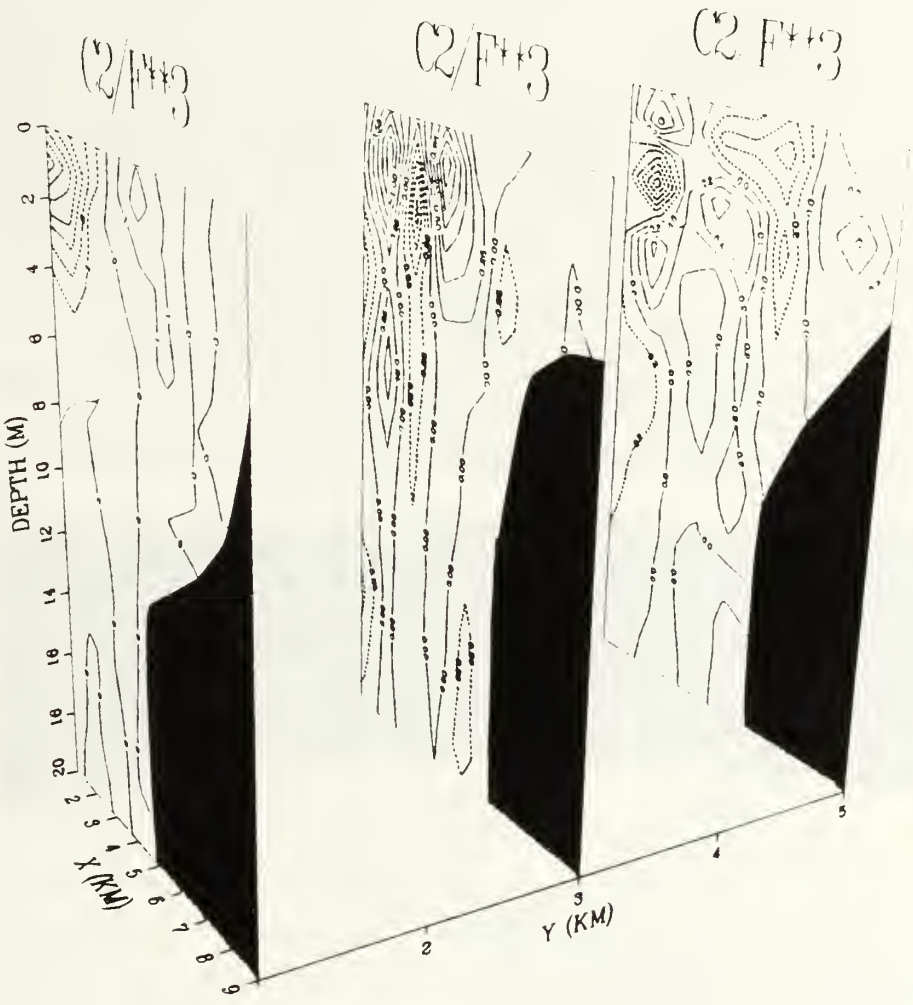

Figure 23. C_2/f^3 values at sections (from left to right) E,C and A.

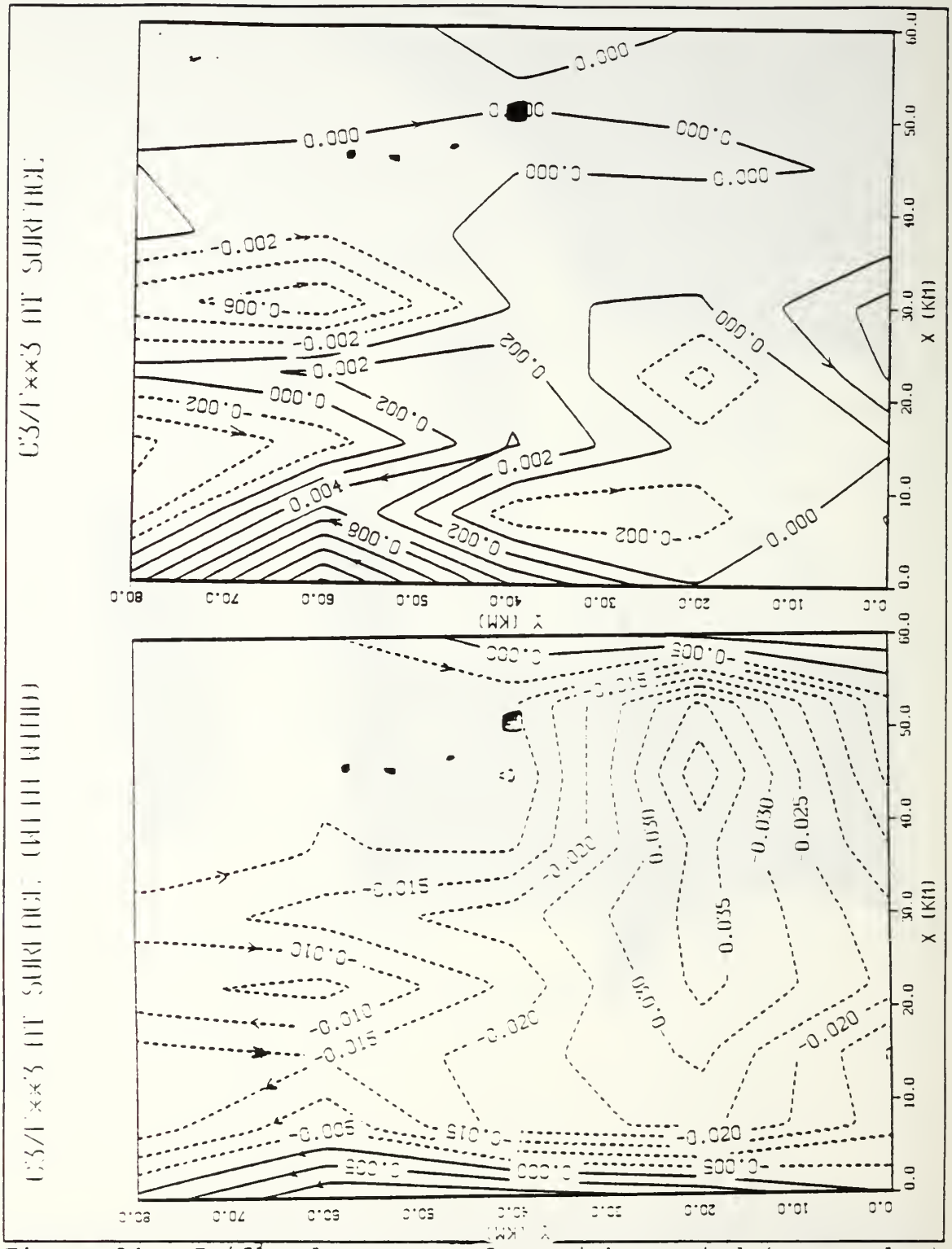

Figure 24. C_3/f^3 values at surface without wind (upper plot) and with wind (lower plot).

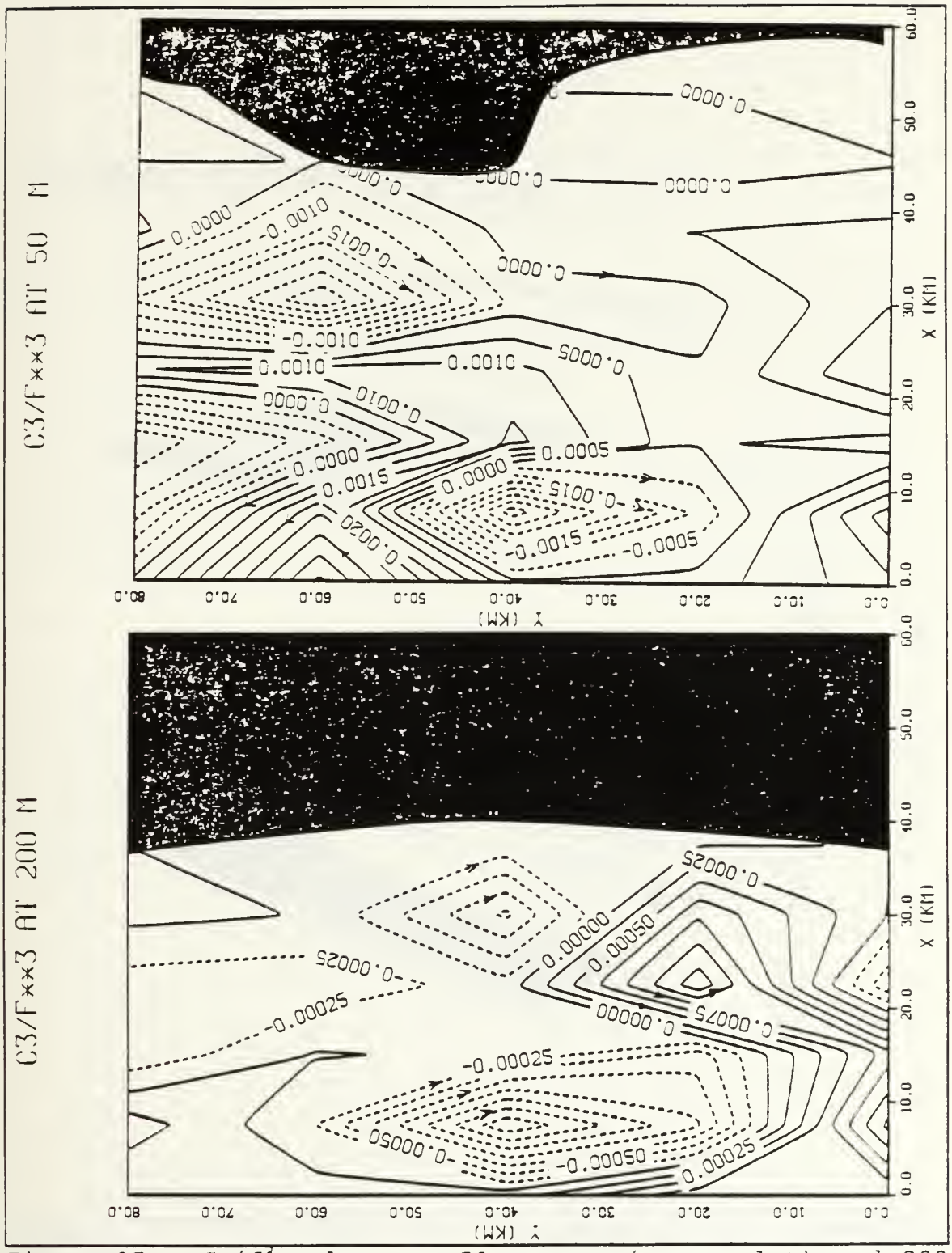

Figure 25. C_3/f^3 values at 50 meters (upper plot) and 200 meters (lower plot).

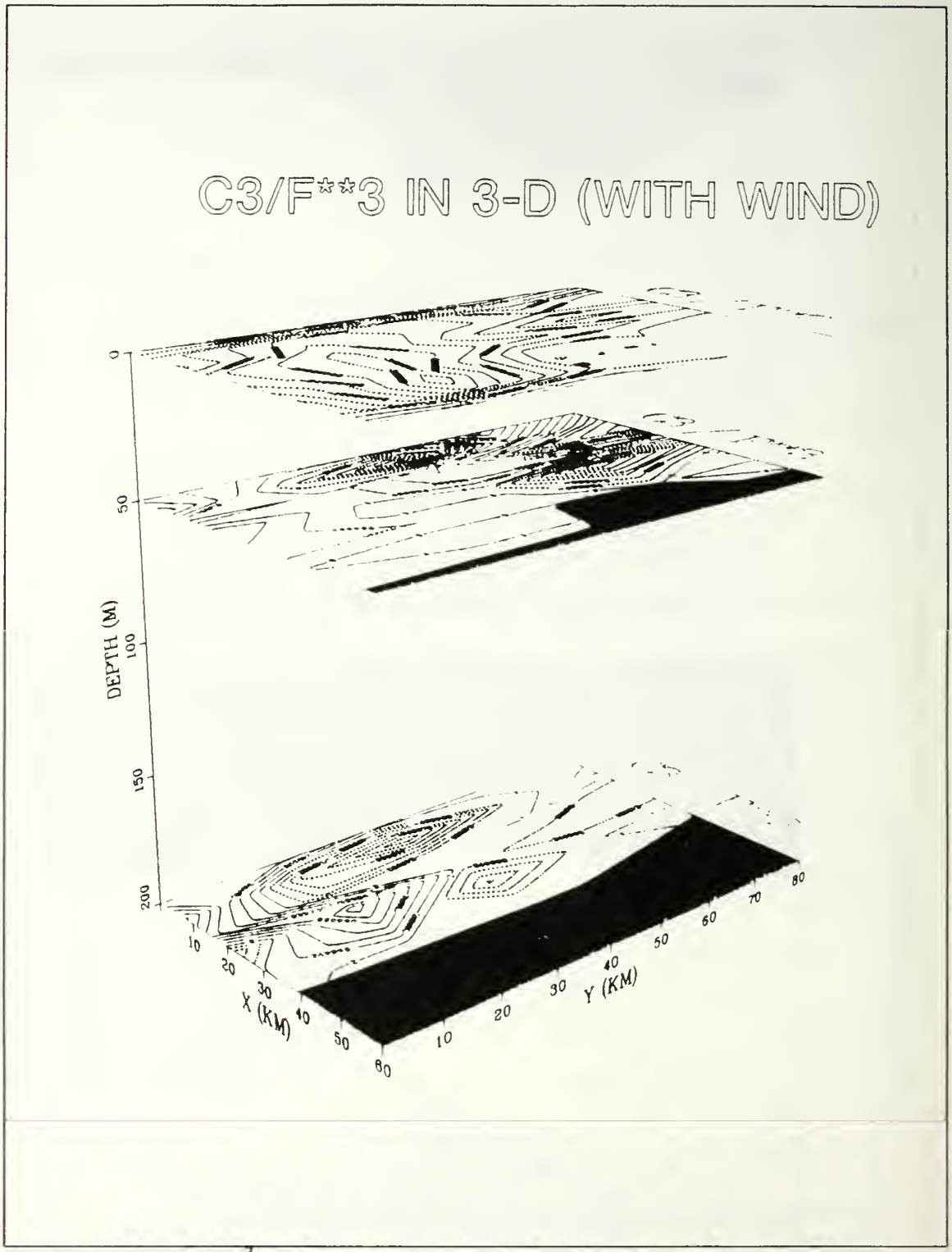

Figure 26. C_3/f^3 values at three layers (surface, 50 meters and 200 meters).

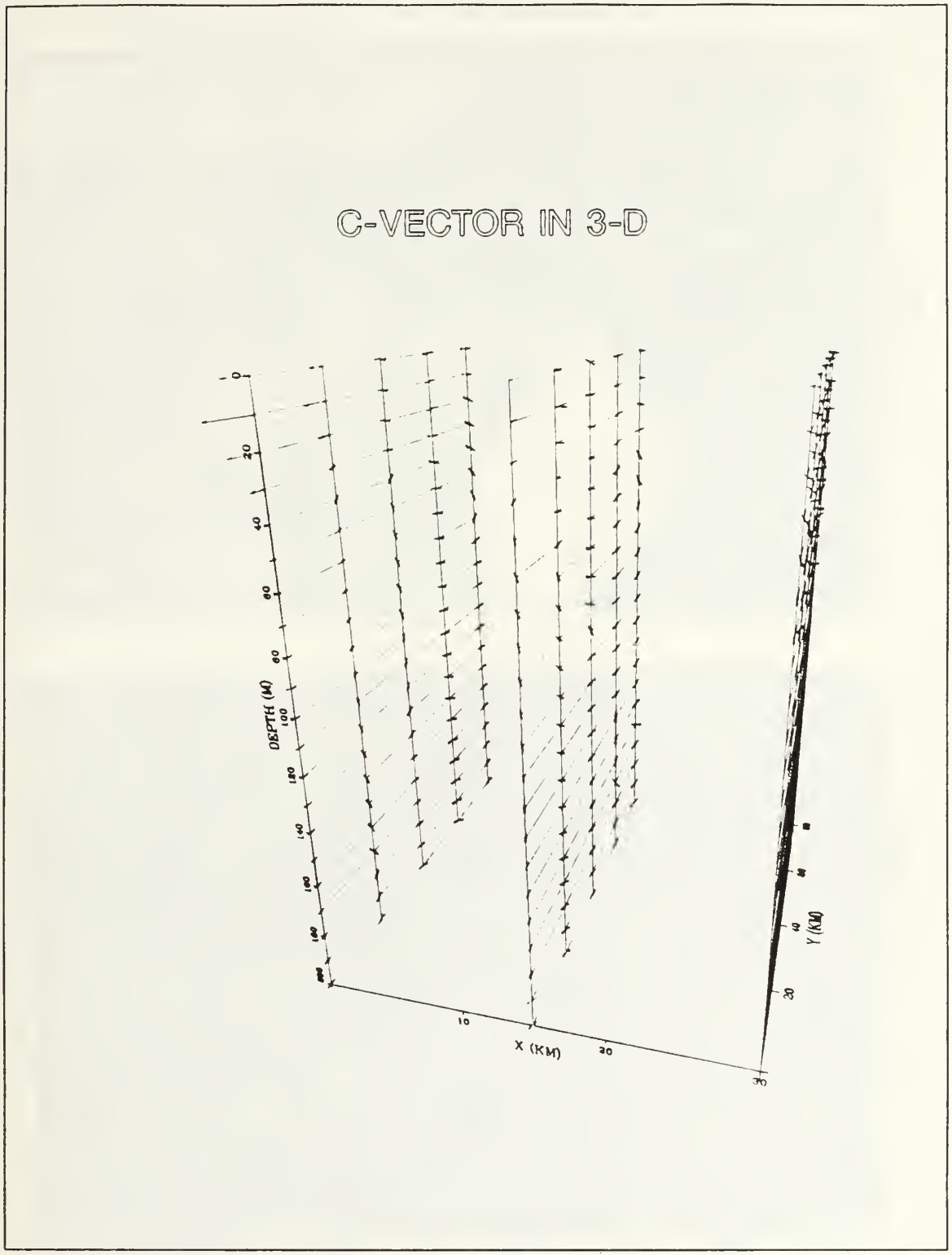

Figure 27. C-Vectors (for ageostrophic circulation) at columns 9,8 and 7.

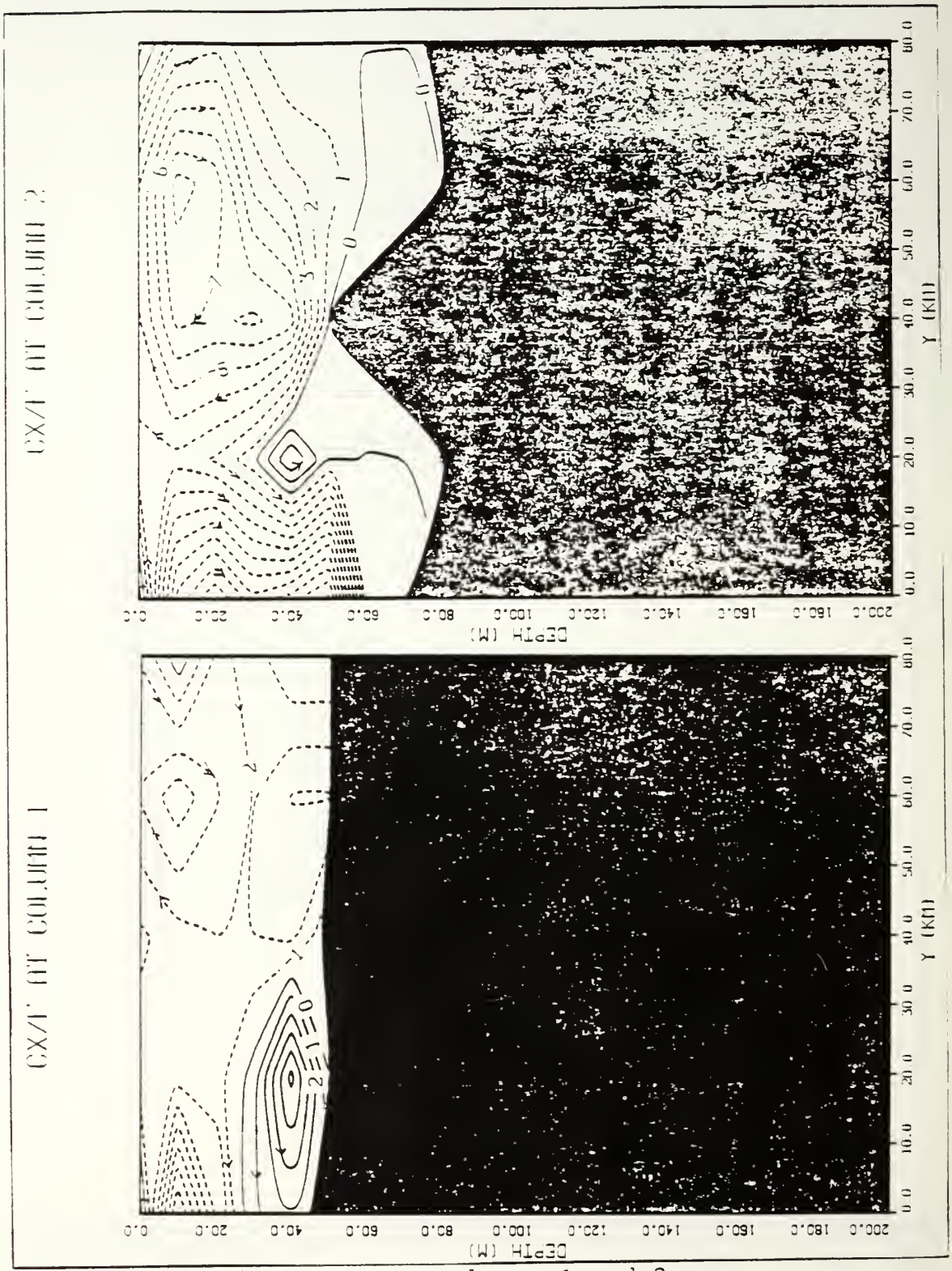

Figure 28. C_x/f values at columns 1 and 2.

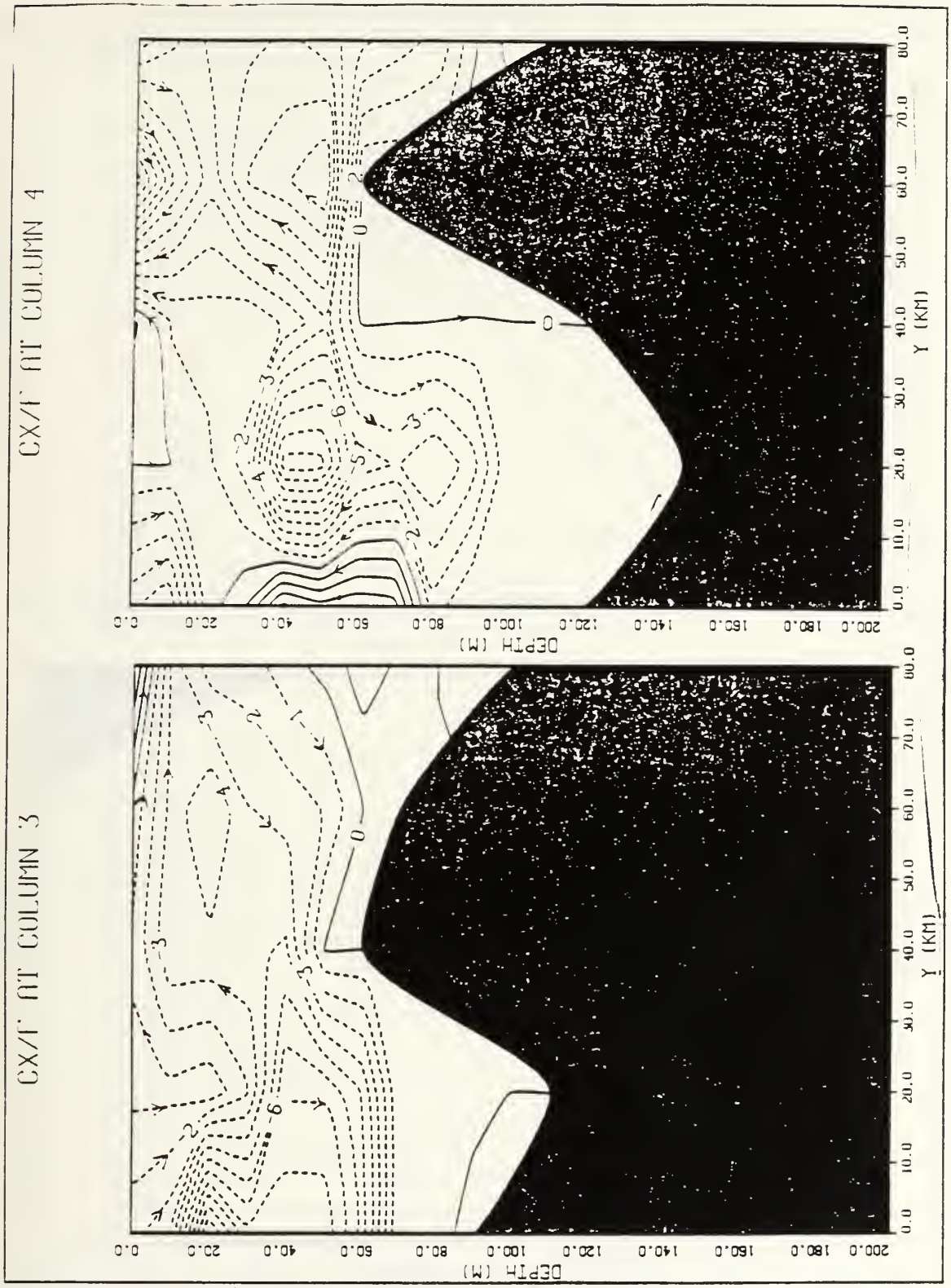

Figure 29. C_x/f values at columns 3 and 4.

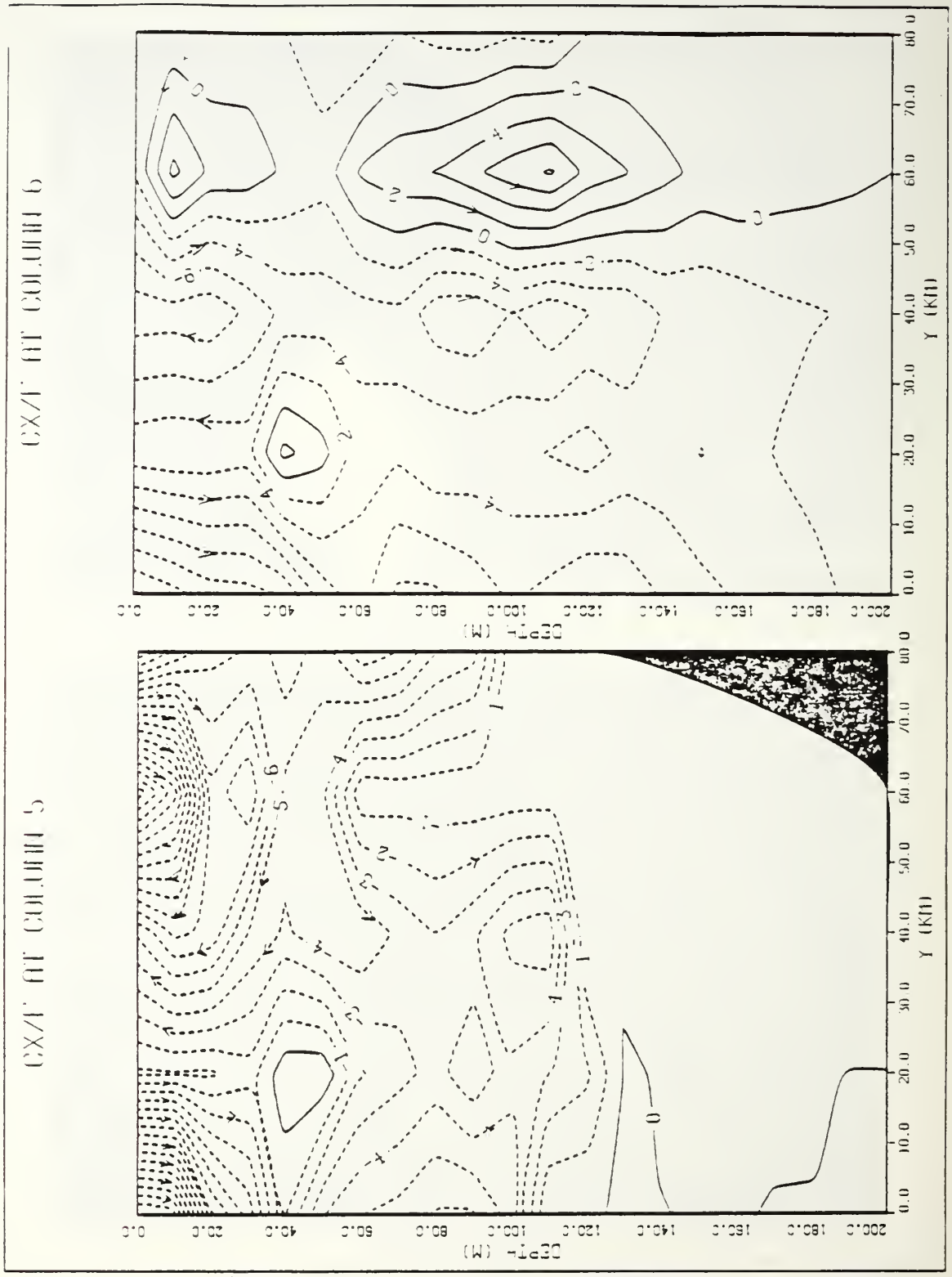

Figure 30. C_x/f values at columns 5 and 6.

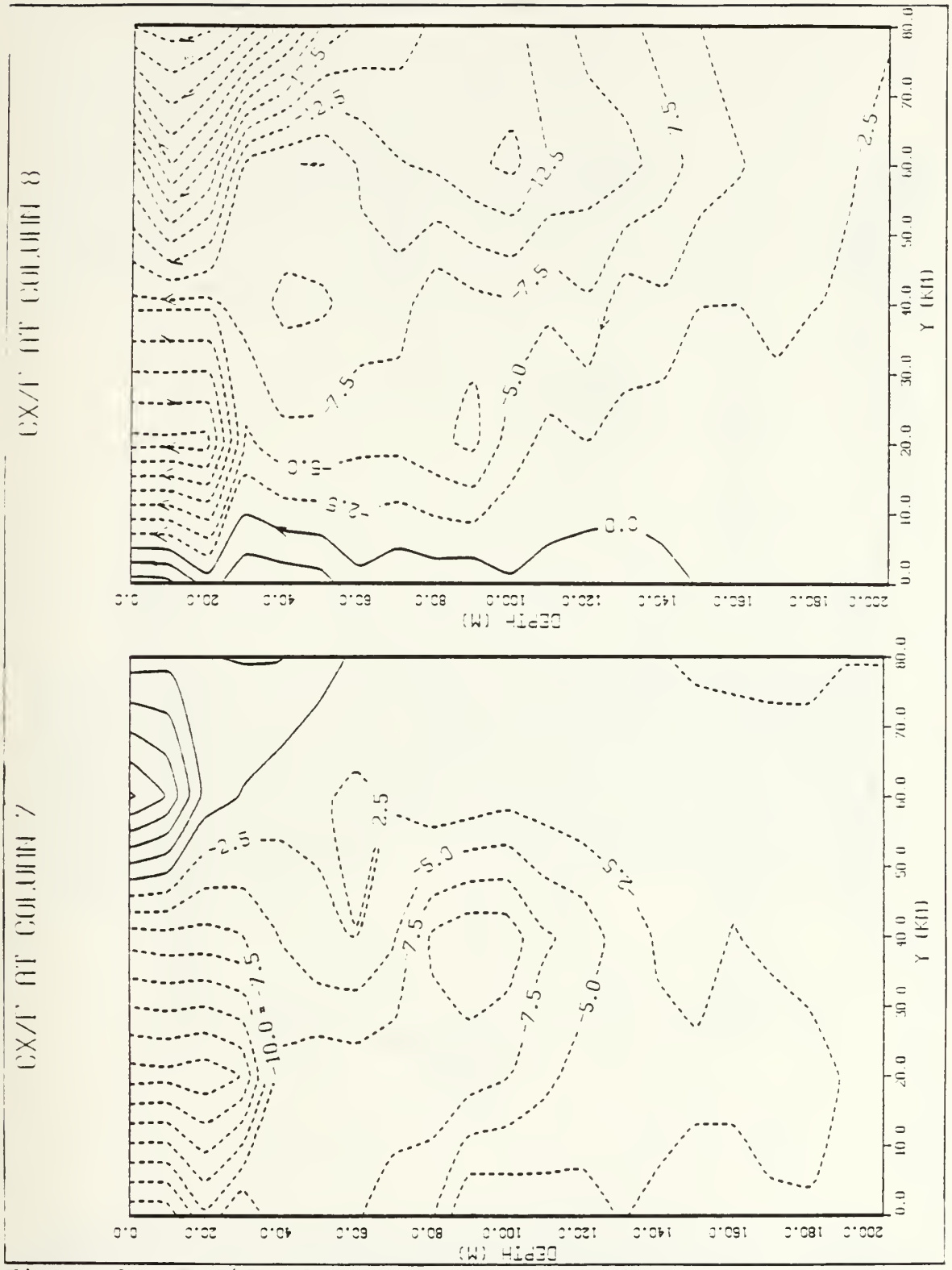

Figure 31. C_x/f values at columns 7 and 8.

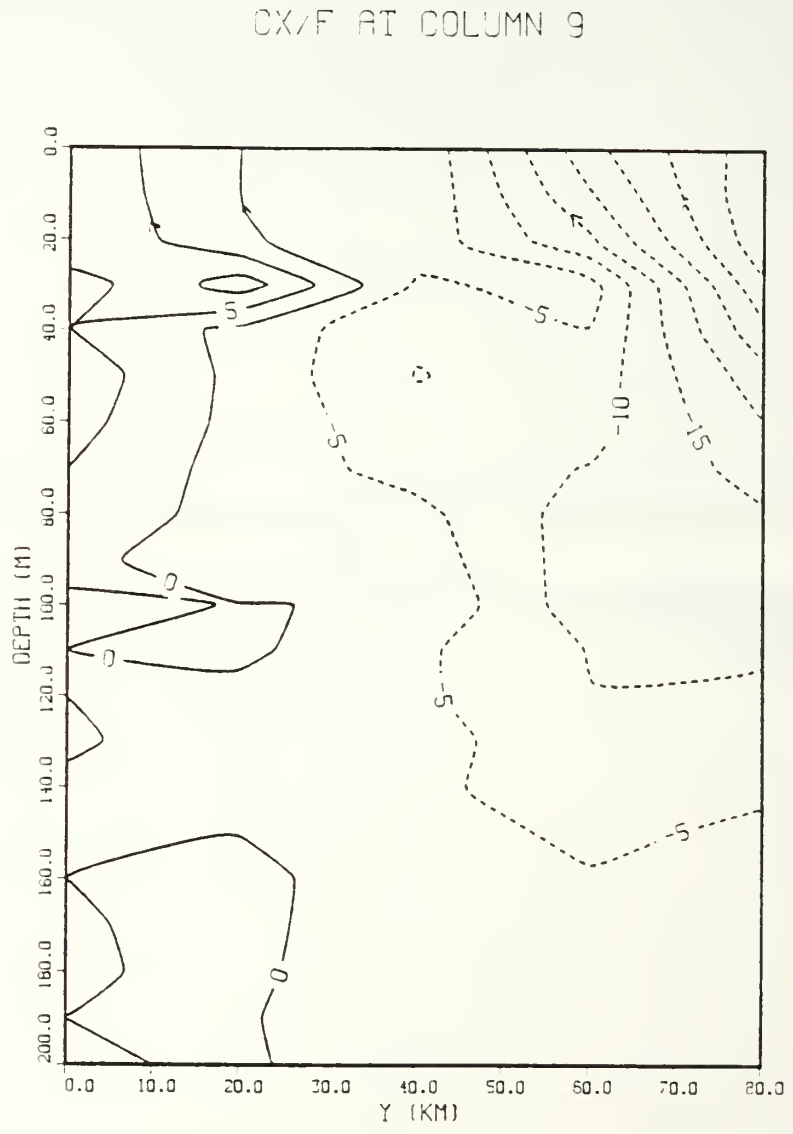

Figure 32. C_x/f values at columns 9.

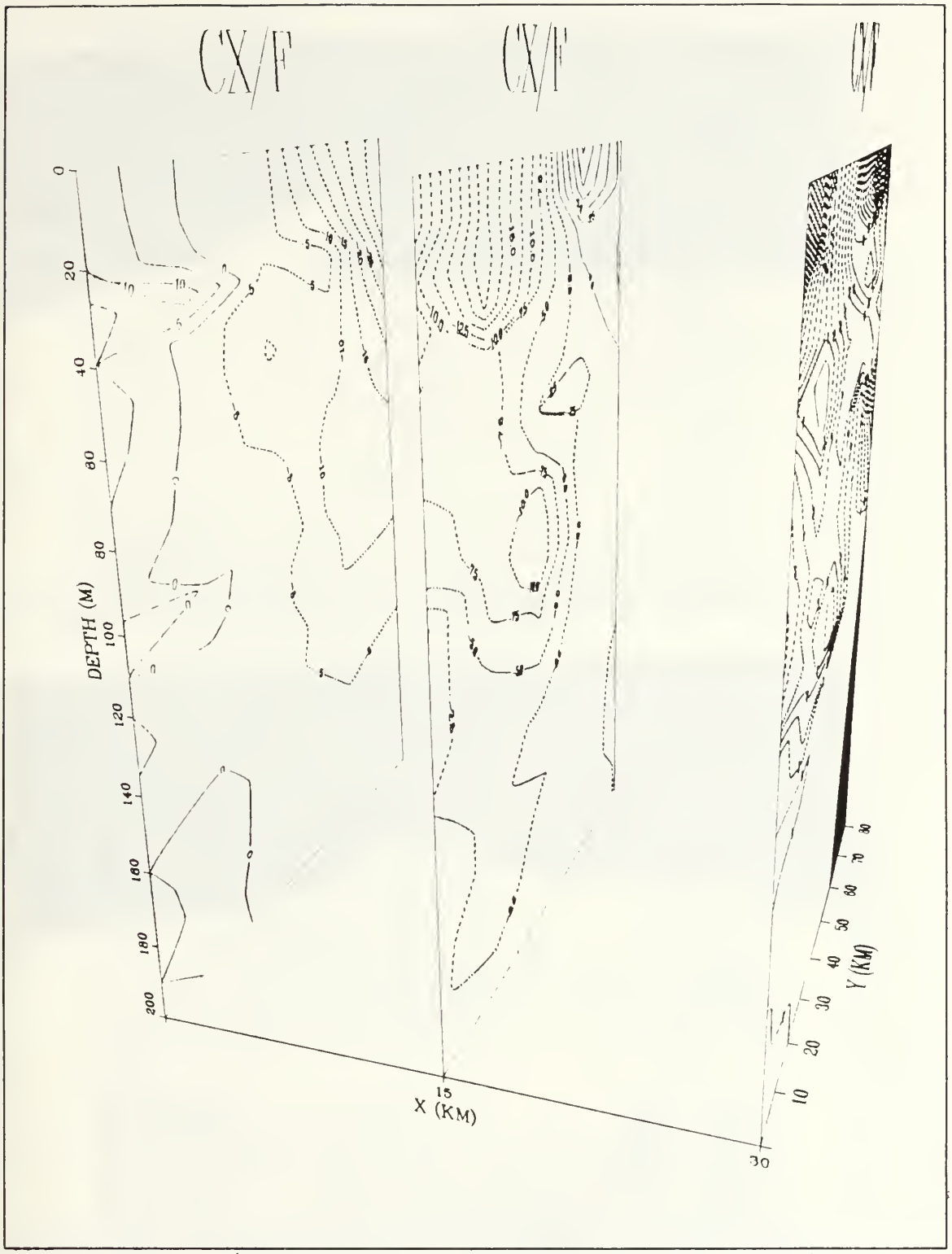

Figure 33. C_x/f values at columns (from left to right) 9,7 and 5.

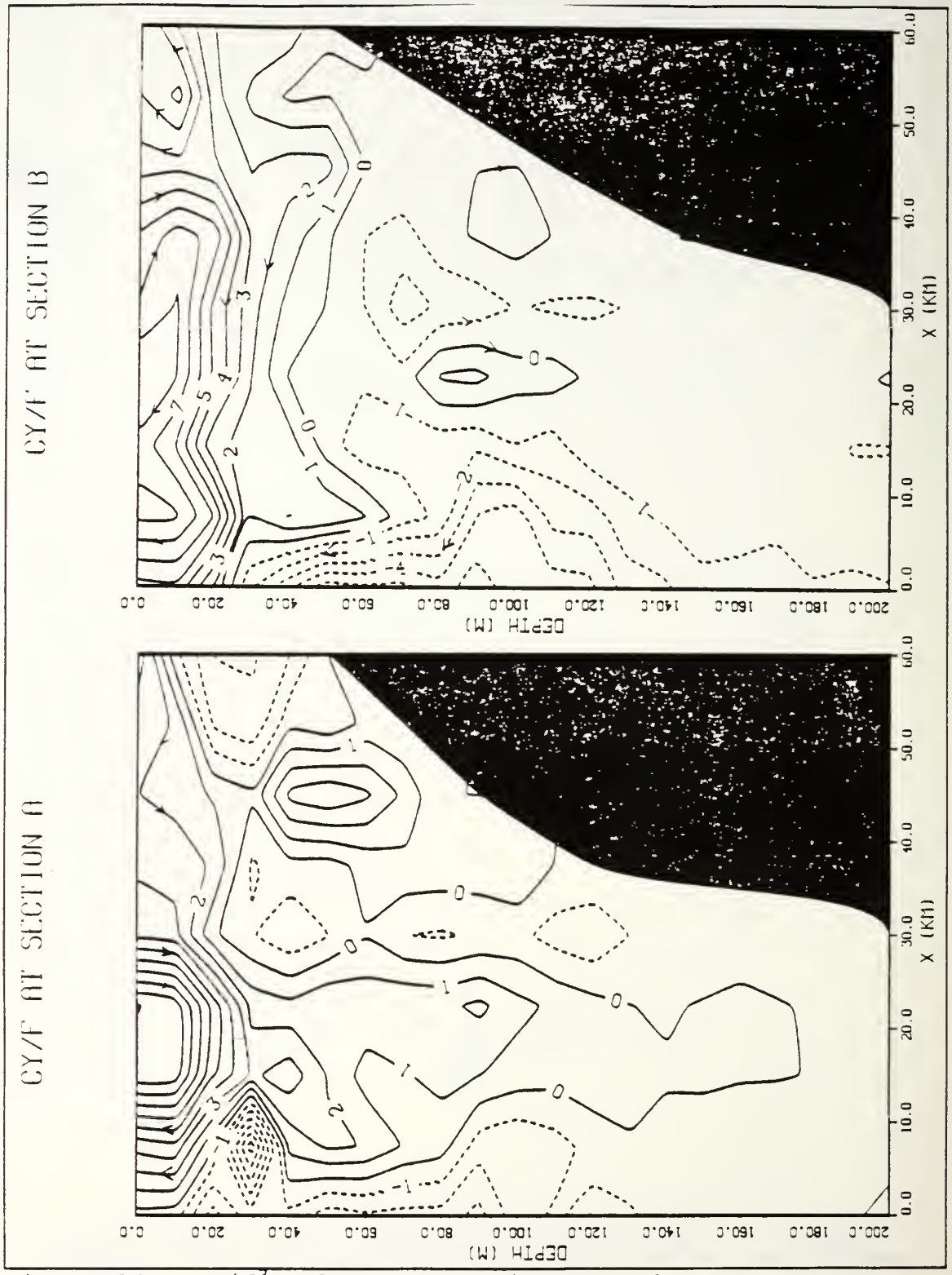

Figure 34. C_y/f^3 values at sections A and B.

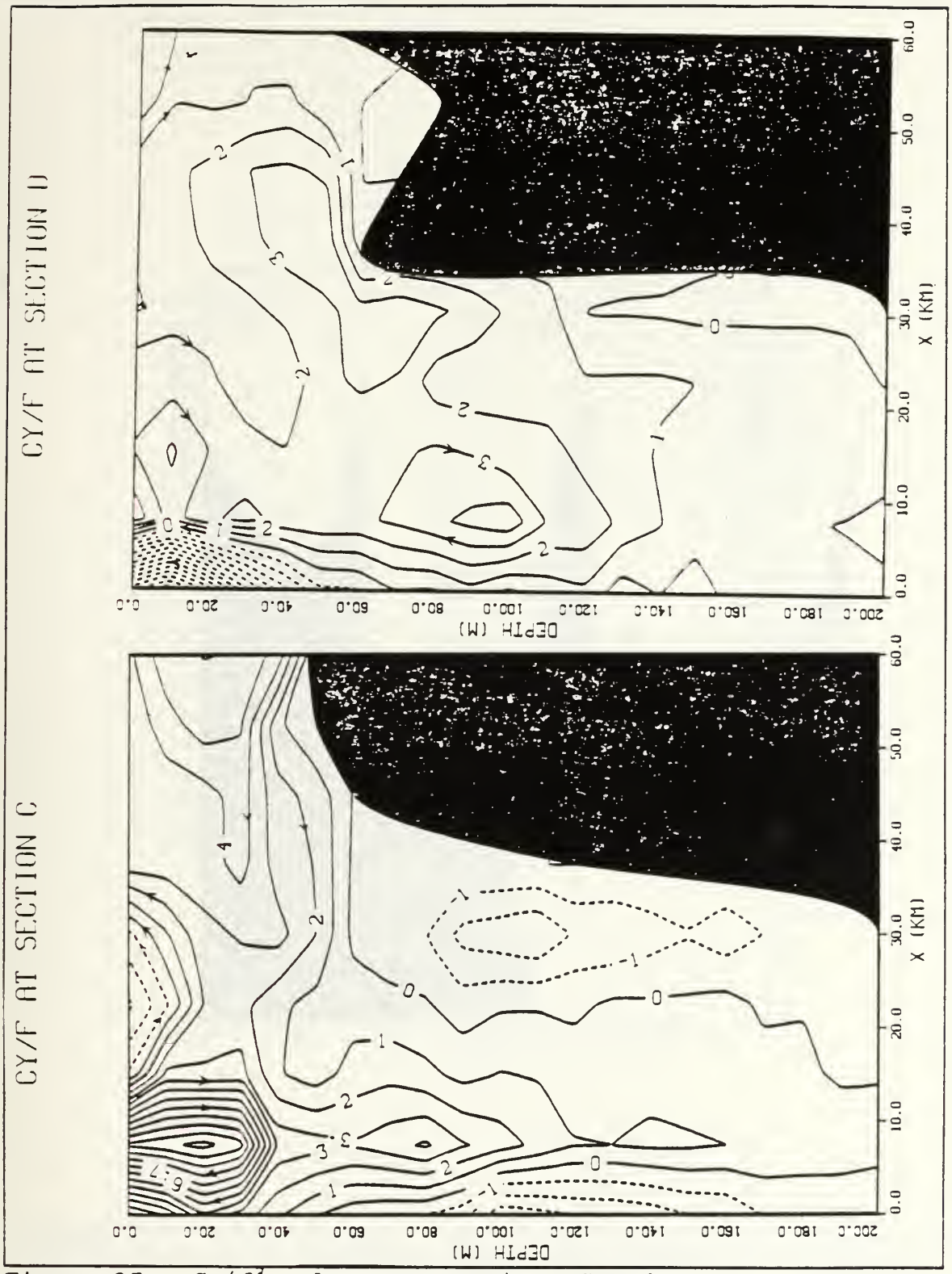

Figure 35. C_y/f^3 values at sections C and D.

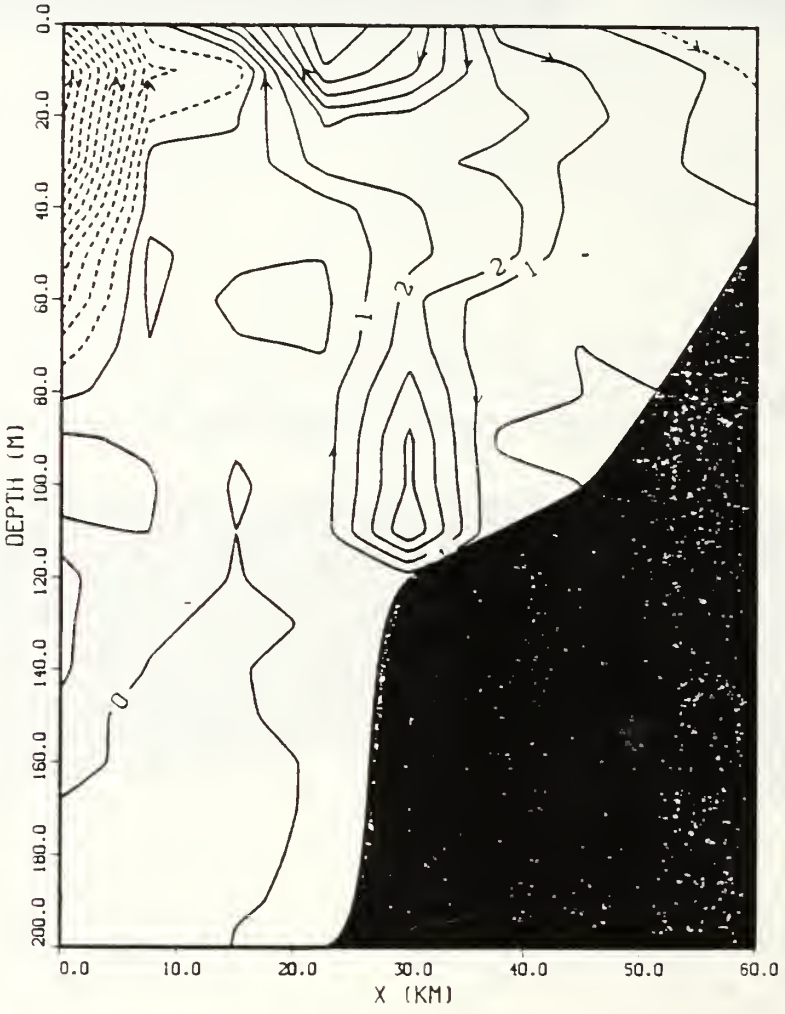

Figure 36. C_y/f^3 values at section E.

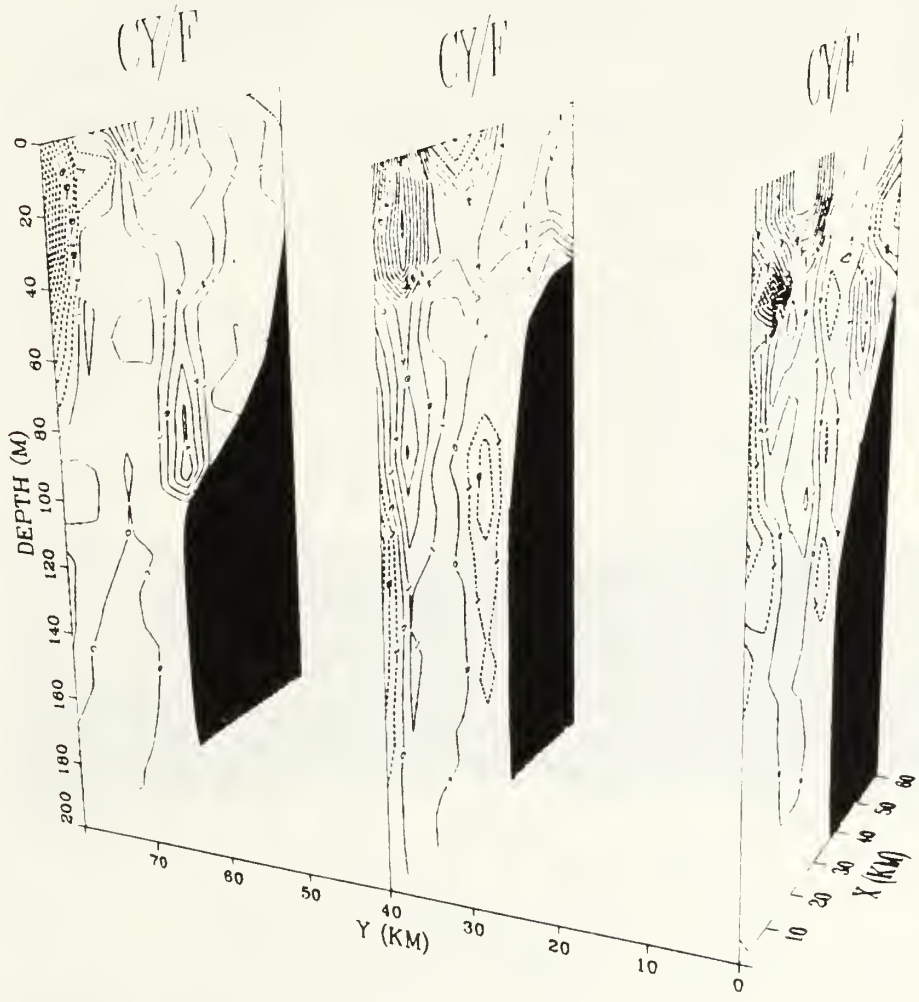

Figure 37. C_y/f^3 values at sections (from left to right) E,C and A.

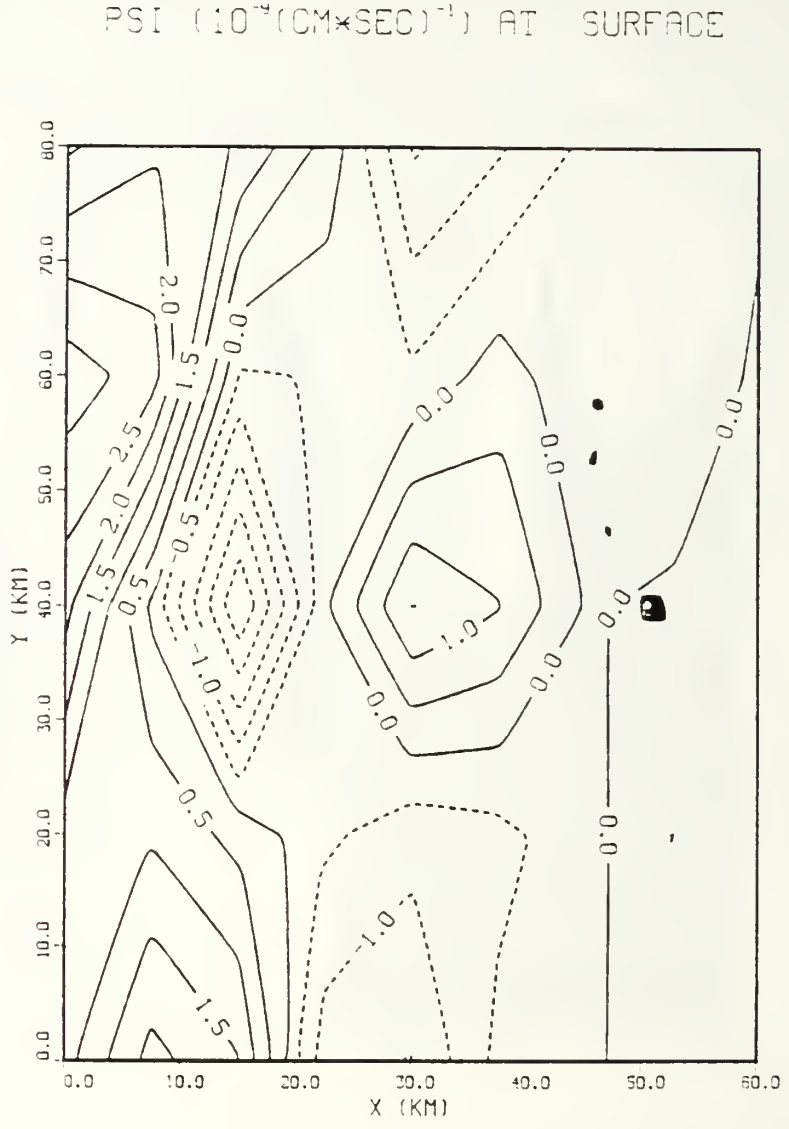

Figure 38. Ψ at surface.

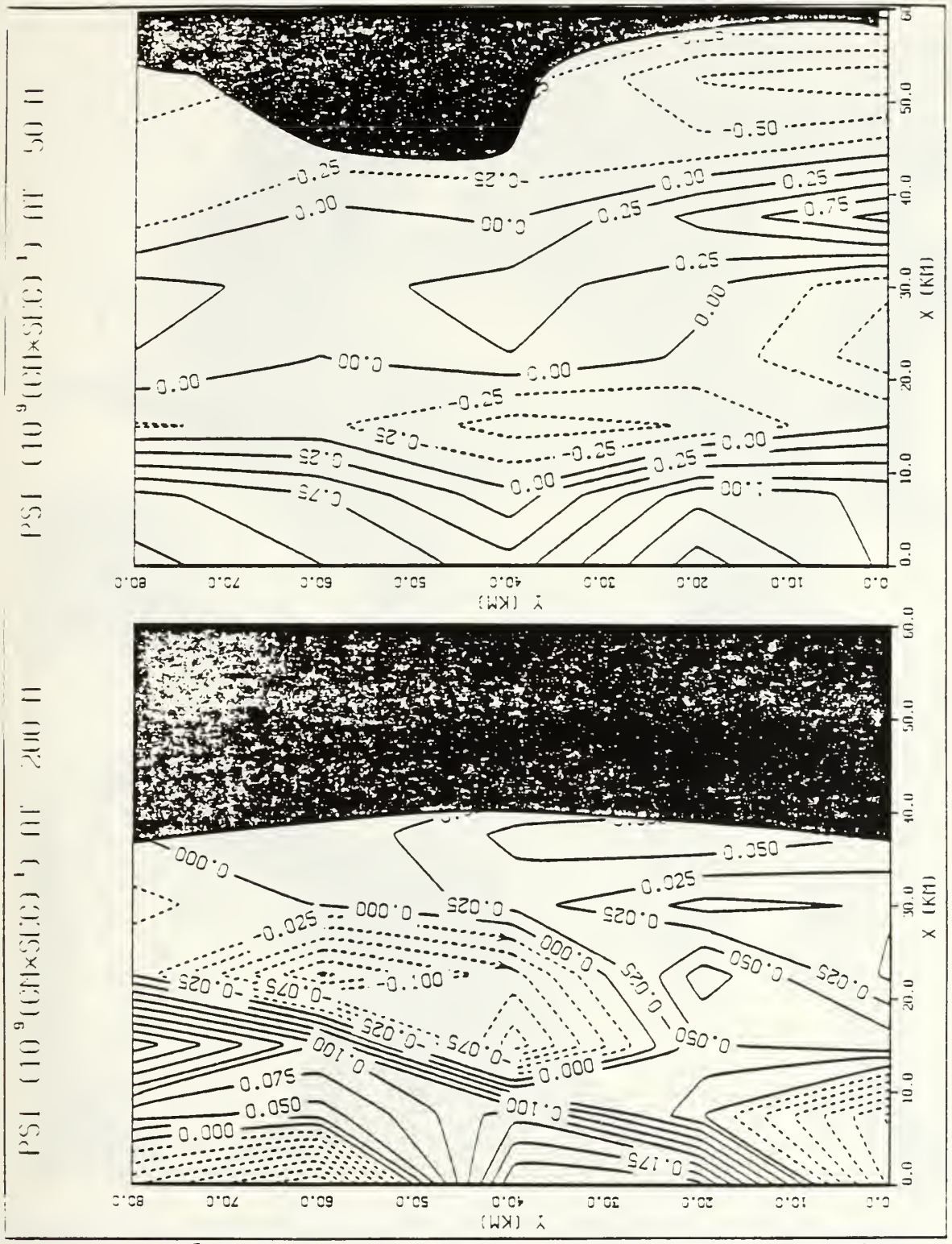

Figure 39. Ψ at 50 meters (upper plot) and 200 meters (lower plot).

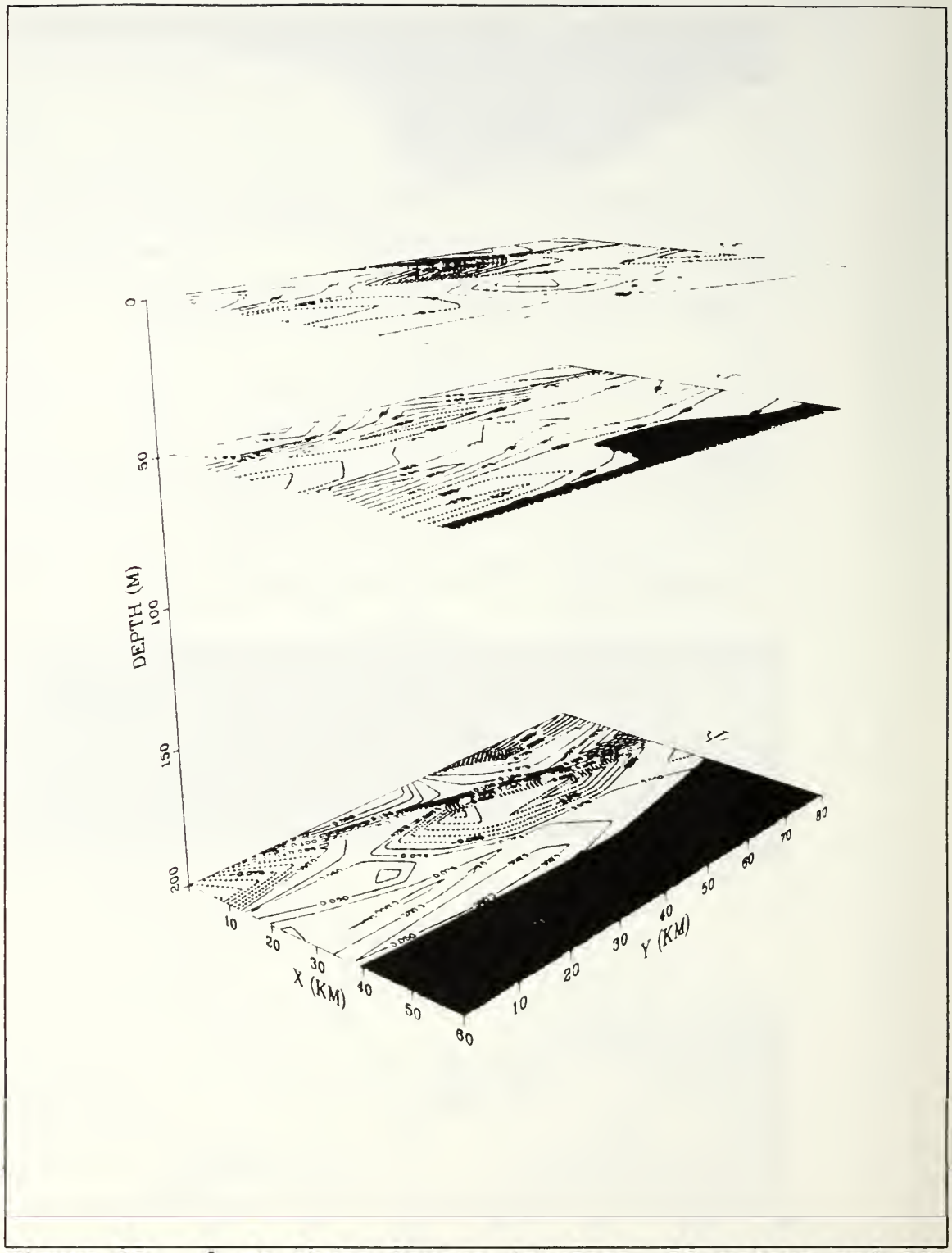

Figure 40. Ψ at three layers (surface, 50 meters and 200 meters).

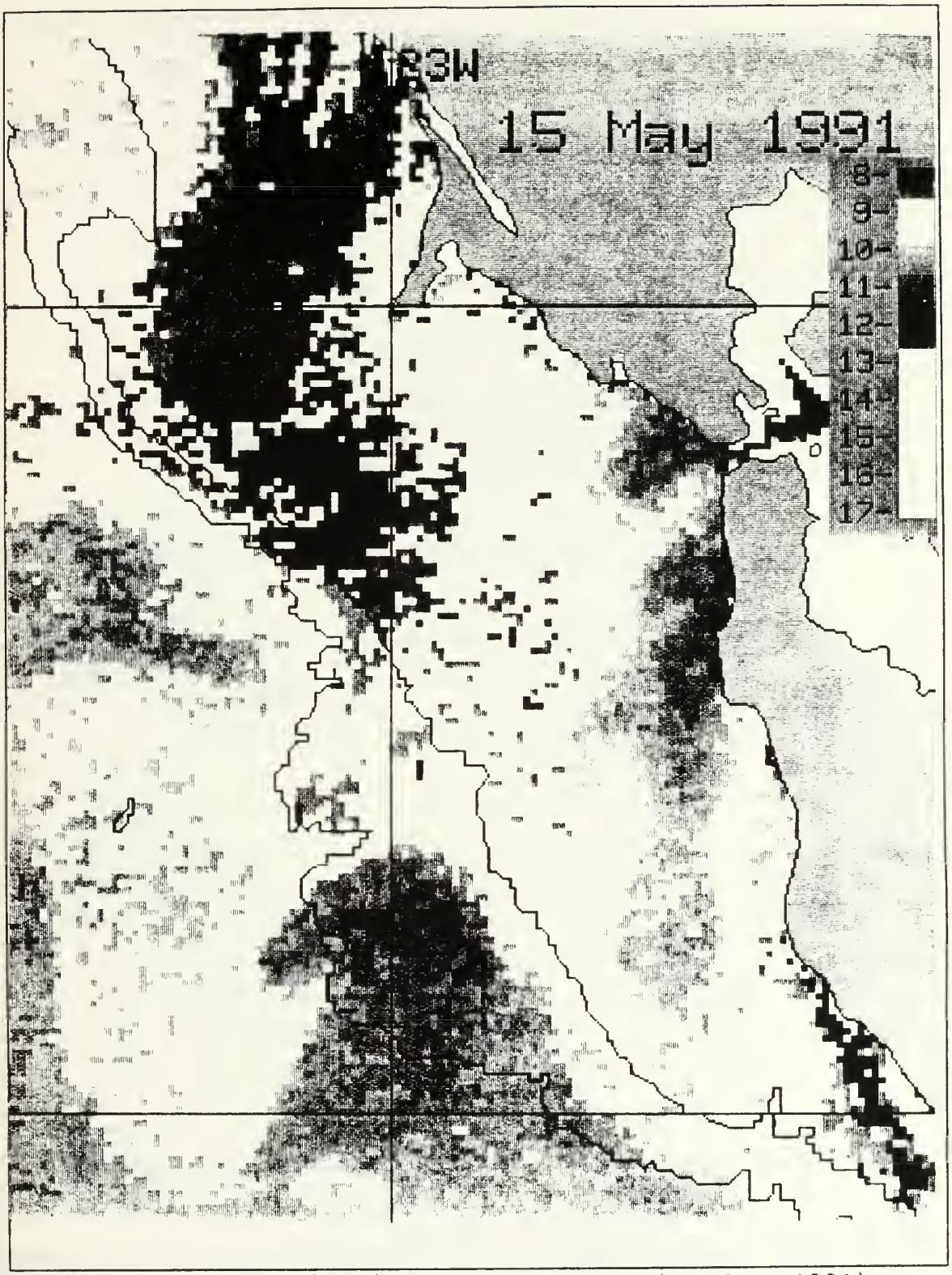

Figure 41. A satellite image of the area (15 May, 1991).

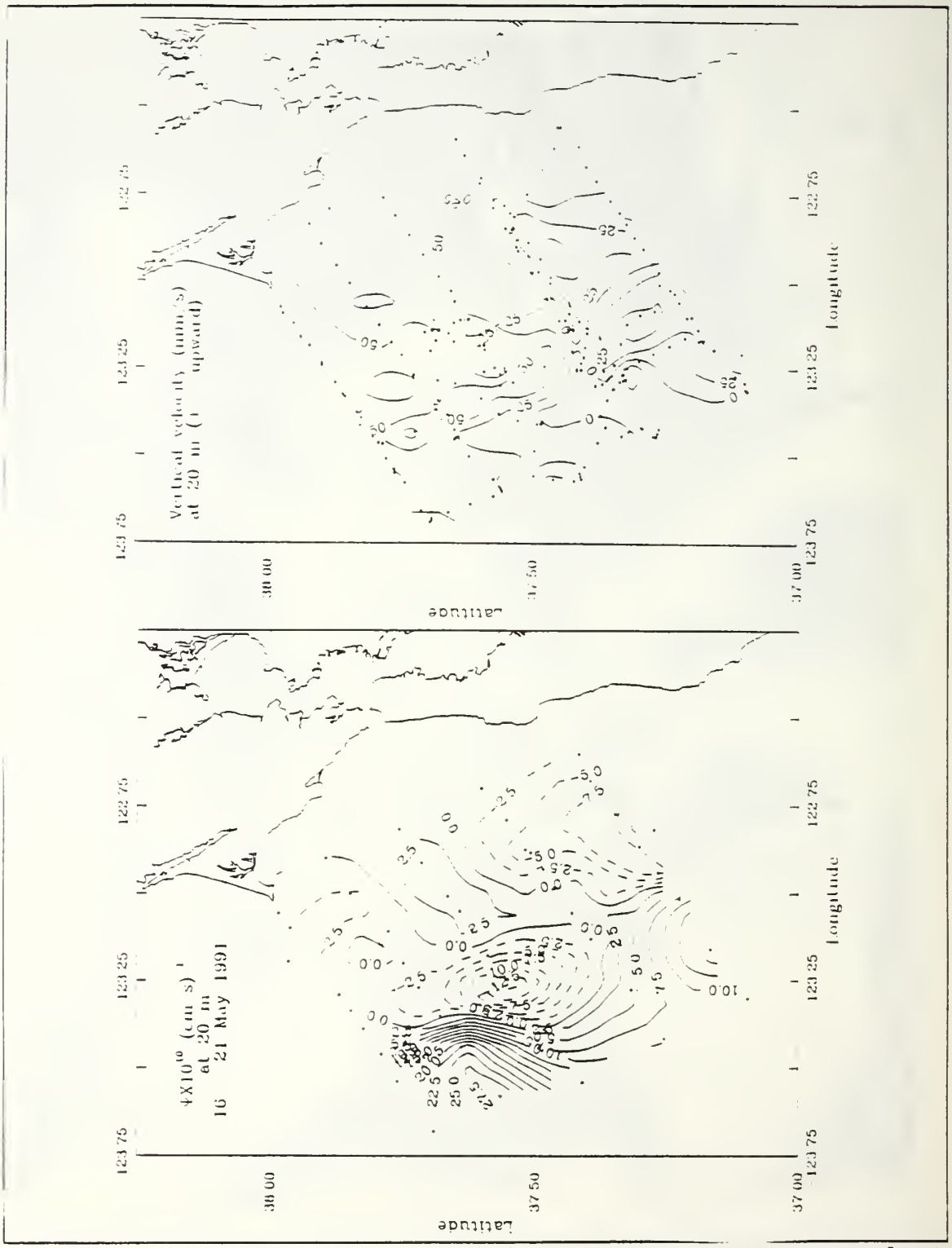

Figure 42. Vertical ADCP velocities at 20 meters (upper plot) and Ψ function at 20 meters (lower plot).

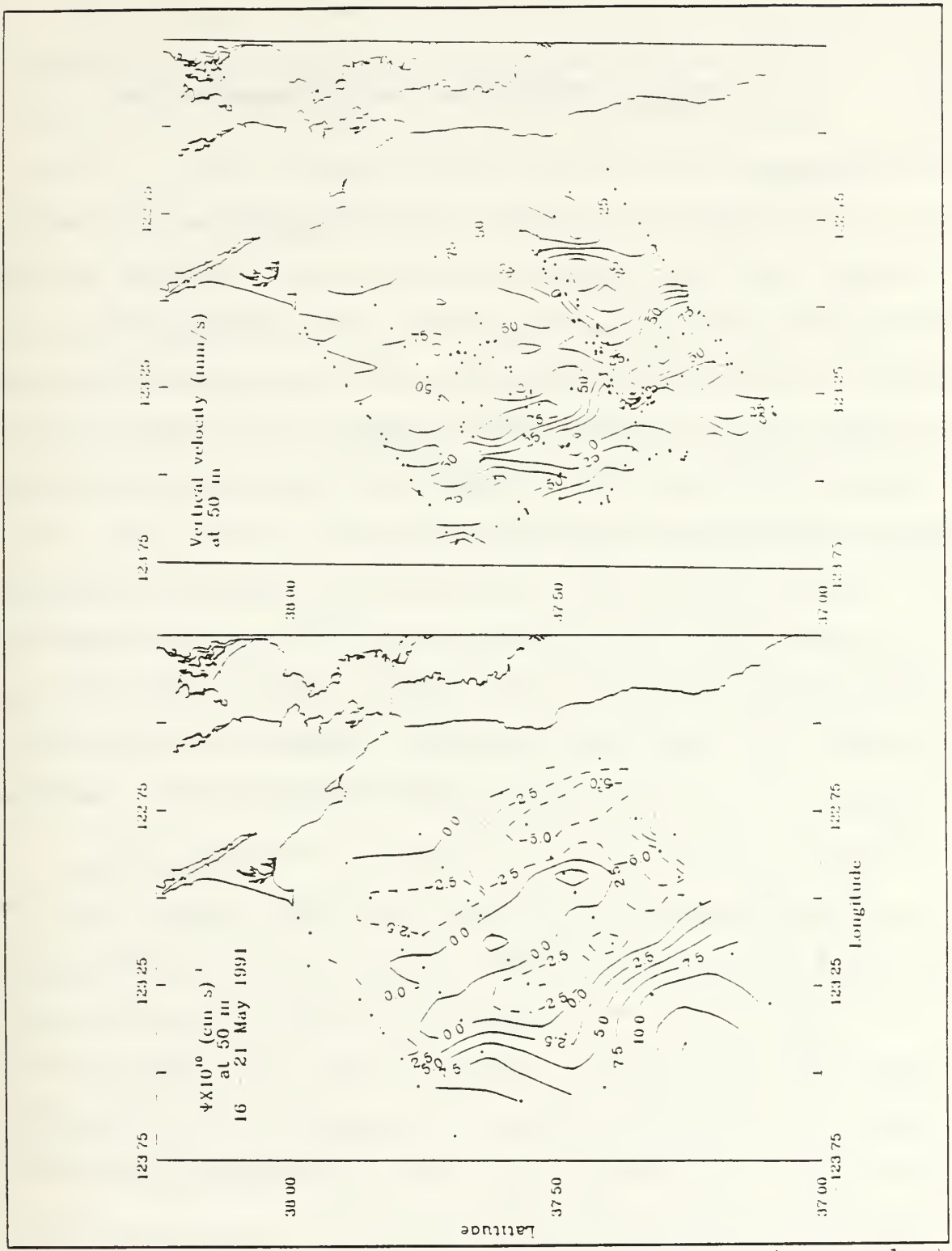

Figure 43. Vertical ADCP velocities at 50 meters (upper plot) and Ψ function at 50 meters (lower plot).

V. SUMMARY, CONCLUSIONS AND RECOMMENDATIONS

A. SUMMARY

The purpose of this study was to demonstrate the C-Vector method and the potential value of this method in the calculation of the ageostrophic circulation using CTD and wind data. Sometimes the ageostrophic flow is significant and the purpose of this study is to emphasize the importance of ageostrophic circulation in waters off California as inferred by C-Vector using CTD and wind data.

Spring is an upwelling season for waters off northern California. The SST satellite image of the area shows two filaments of cold water. One extends west of the Farallones islands and the other stretches offshore of the 1,000 m isobath. The cold filaments are associated with positive values of the vorticity of C-Vector Ψ (equation (29)).

The main upwelling extends to a depth of 200 m, and the strong C-Vector cells extend from the surface to about 200 m. Cells below 200 m are observed to be very weak. This is in phase with the Sverdrup assumption that the upwelling water rises from moderate depths only, probably less than 200 m (Sverdrup and Fleming, 1941), and the phenomenon represents overturning of the upper layer.

Some large values of C_1, C_2 and C_x, C_y (horizontal components of C-Vector for the ageostrophic and the total circulation) are found over the continental slope. This probably occurs because of the presence of the continental slope and is associated with oceanic processes which occur there.

A shortcoming in the calculations of C-Vector could be the uncertainty associated with the determination of a reference level. Density differences between stations demonstrate that 1,400 m is the main representative LNM for the deep waters. While the depths where the difference in density between stations is zero are not always 1,400 m, there is a good indication that at this level currents are very small.

The Beta-spiral method (Schott and Stommel, 1978) overcomes the erroneous "level of no motion" and allows the "level" to vary realistically in (x,y).

B. CONCLUSIONS

The C-Vector is a good method for calculating the three-dimensional pseudo-vorticity fields in the ocean using CTD measurements and wind stress data.

This technique (with the help of Ψ) provides some useful information of the upward and downward motions in the ocean.

If the pseudo-vorticity equations can be solved, the three-dimensional circulation in the ocean can be obtained.

C. RECOMMENDATIONS

Data from May 1991 gave a picture of the utility of C-Vector method and the pseudo-vorticity fields at the Gulf of Farallones Islands.

These data are complicated by such local phenomena as upwelling, tides, inertial motions and winds. It is recommended that the results of this study should be compared with:

- The pseudo-vorticity fields using data from other sources, for example from a current meter array covering the area for verification
- Results of other studies and calculations of C-Vector from the same area.

In the future it is also recommended to use the β-spiral method in the C-Vector computation. The advantage of the β-spiral method is that it overcomes the problems of the "level of no motion" and for this reason it is expected to improve the C-Vector method.

Another way to avoid the uncertainty of the level of no motion or the reference level could be the use of satellite altimetry data. This data can be used for the determination of the geostrophic currents at the ocean surface. Then, an integration of the thermal wind equation from surface to a certain depth z can provide the geostrophic velocities at different depths.

LIST OF REFERENCES

Breaker, L., C., and Gilliland, R., P., A Satellite Sequence on Upwelling along the California Coast, Richards, F., A., 1981

Chavez, F., P.,and others, "Horizontal Transport and the Distribution of Nutrients in the Coastal Transition Zone off Northern California: Effects on Primary Production, Phytoplankton Biomass and Species Composition",Journal of Geophysical Research, v. 96,no. C8, pp. 14,833-14,844, 15 August, 1991

Chelton, D., B, Seasonal Variability of Alongshore Geostrophic Velocity off Central California,J. Geophys. Res. 89, pp. 3,473 - 3,486, 1984

Chelton, D., B., Bernstein, A., W., Bratcovich and Kosro P., M., The Central California Circulation Study, EOS Transactions, American Geology Union vol. 68, no. 1, 6 January, 1987

Chelton, D., B., and others, "Poleward Flow off California during the Spring and Summer, Journal of Geophysical Research, vol. 93, no. C9, pp. 10,604-10,620, 15 September, 1988

Chu, P.,C., Three Dimensional Eastern Greenland Sea Circulation Computed from a CTD Data Set",ARCSS Ocean-Atmosphere-Ice Interactors, NSF, pp. 61 - 64, 1992

Chu, P., C., Three Dimensional Pseudo-Vorticity Fields in the West Spitzbergen Current, Pollar Meteorology and Oceanography, vol. III, pp. 101 - 104, 1992.

Collins, C., A., Summary of Hydrographic Conditions in the Region of the Farallones from 16-21 May 1991, unpublished document, Naval Postgraduate School, Monterey, Ca, 1992

Conomos, T., J., San Francisco Bay, The Urbanized Estuary, Pacific Division of the American Association for the Advancement of Science, pp. 493, 1979

Crowe and Schwartzlose, Release and Recovery Records of Drift Bottles in the California Region 1955 through 1971, California Cooperative Oceanic Fisheries Atlas # 16, Marine Research Committee, State of California, 1955

Defant, A., Vol. I Physical Oceanography, Pergamon Press, 1961

Fofonoff, N., P., Physical Properties of Seawater, J. Geophys. Res. 90, pp. 3,332 - 3,342, 1985

Fomin, L., M., The Dynamic Method in Oceanography, Elsevier, 1964

Hickey, B., M., The California Current System - Hypothesis and Facts, Progr. Oceanogr., vol. 8, pp. 191 - 279, 1979

Hickey, B., M., The California Current System - Hypothesis and Facts, Progr. Oceanogr., vol 93 , no. C9, pp. 10,604 - 10,620, 15 September, 1988

Hoskins, B., J., Draghich I. and Davies H., C., A New Look at the Ω - equation, Quart. J. Roy. Meteor. Soc., 104, 31 - 38, 1978

Huyer, A., Coastal Upwelling in the California Current System, Prog. Oceanogr., vol. 12, pp. 259 - 284, 1983

Huyer, A., Pillsbury and Smith R., L., Seasonal Variation of the Along Shore Velocity Field Over the Continental Shelf off Oregon, limnology and Oceanography, 20, pp. 90 -95, 1975

Huyer, A., Smith, R., L. and Sobey E., J., C., Seasonal Differences in Low Frequency Current Fluctuations Over the Oregon Continental Shelf, Journal of Geophysical Research, 83, pp. 5,077 - 5,089, 1978

Jessen P., Collins C., A., Ramp S., R., Garfield N., Rosenfeld L., K. and Schwing F., B., Hydrographic and Acoustic Doppler Current Profiler (ADCP) Data from the Farallones Shelf and Slope Study 16-21 May 1991, NPS technical report NPS-OC-92-004, 1992

Kosro, P., M. and others , "The Structure of the Transition Zone Between Coastal Waters and the Open Ocean off Northern California, Winter and Spring 1987", Journal of Geophysical research, v. 96, no. C8, pp. 14,707 - 14,730 , 15 August 1991

Kosro, P., M., Shipboard Acoustic Doppler Current Profiling During the Coastal Ocean Dynamics Experiment, Ph.D. Dissertation , SIO Ref 85 - 8, Scrips Institution of Oceanography, 1985

Mamaev, O., I., Methods of Determining the Zero Dynamic Surface in the World Ocean. Vest. Mosk. Univ., no. 10, 1955

Pond, S. and Pickard, G., Introductory Dynamic Oceanography, Pergamon Press, 1961

Pond, S. and Pickard, G., Introductory Dynamic Oceanography (2nd edition), Pergamon Press, 1986

Ramp S., R., Garfield N., Collins, C., A., Rosenfeld L., K. and Schwing F., B., Circulation Studies Over the Continental Shelf and Slope near the Farallones Islands, Unpublished document, NPS, 1992

Reid, J., L., Roden G., I. and Wyllie J., G., Studies of the California Cooperative Oceanic Fisheries Investigations Progress Report , 7-1-56 to 1-1-58, Marine Resources Committee, California Department of Fish and Game, Sacramento, 27 - 56, 1958

Schott, F. and Stommel, H., Beta - spirals and absolute velocities in different oceans, Deep Sea Research, 25, pp. 961 - 1010, 1978

Schwartzlose, R., A., Nearshore currents of the Western United States and Baja California as measured by Drift Bottles, California Cooperative Oceanic Fisheries Investigations Progress Report, Marine Research Committee, California Department of Fish and Game, Sacramento, Ca, 1963

Shepard, F., P., Marshall N., F., McLoughlin P., A., Sullivan G., G., Currents in Submarine Canyons and Others Seavalleys, American Association of Petroleum Geologists (AAPG) studies in Geology, no., 8, 1979

Shepard, F., P., Submarine Topography off the California Coast, Geological Society of America, no. 31, 28 May 1941

Stetson, H., C., Geology and Paleontology of the Georges Bank Canyons, part 1, Geology, Geol. Soc. America Bull, v., 47, pp. 339 - 366, 1936

Sverdrup H., U. and Flemming R., H., The Waters Off the Coast of Southern California, March to July, 1937, scrips Inst. Oceanogr., Bull., v. 4, no. 10, pp. 261 - 378, 1941

Sverdrup, H., U., Johnson M., W. and Fleming R., H., The Oceans, Prentice - Hall, INC, November, 1964

Soule, F., M., Consideration of the Depth of the Motionless surface near the grand Banks of new - foundland, woods Hole Oceanogr. Inst. Coll. Rept., Contrib., 230, 1939

Sutcliffe, R., C., A Contribution to the Problem of Development, quart. J. Roy., Meteor. Soc. 73, pp. 370 - 383, 1947

Tibby, R., B., The Water masses off the West Coast of North America, Journal of Marine Research, vol. 4, pp. 112 - 121, 1941

Wyatt, B., Bort, W., V. and Pattullo J., G., Surface Currents off Oregon as Determined from Drift Bottles Returns, Journal of Physical Oceanography, v. 2, pp. 286 - 293, 1972

Xu, Q., Ageostrophic Pseudovorticity and Geostrophic C-Vector Forcing a new look at the Q-Vector in three dimensions, Journal of Atmospheric Science, 49, 981 - 990, 1992

Yoshida, K., Circulation in the Eastern Tropical Oceans with special references to upwelling and Undercurrents, Japanese of Geophysics, 4, 1 - 75, 1967

INITIAL DISTRIBUTION LIST

		No. Copies
1.	Defense Technical Information Center Cameron Station Alexandria VA 22304-6145	2
2.	Library, Code 052 Naval Postgraduate School Monterey CA 93943-5002	2
3.	Chairman (Code OC/Co) Department of Oceanography Naval Postgraduate School Monterey, CA 93943	1
4.	Dr. P. C. Chu, (Code OC/Cu) Department of Oceanography Naval Postgraduate School Monterey, CA 93943	1
5.	Dr. R. W. Garwood, (Code OC/Gd) Department of Oceanography Naval Postgraduate School Monterey, CA 93943	1
6.	Embassy of Greece Naval Attache 2228 Massachusetts Av. NW Washington DC 20008	2
7.	U. S. Environmental Protection Agency 75 Hawthorne Street San Francisco, CA 94105	1
8.	Farallones National Marine Sanctuary Fort Mason San Francisco, CA 94123	1
9.	Library Scripps Institution of Oceanography P. O. Box 2367 La Jolla, CA 92037	1

10. Hydrographic Service 1
Athens BST 902
Greece

11. Simon Konstantinidis 2
Archimidou 42 T.K. 18451
Piraeus Greece